修　士　論　文

Applications of Compressed Sensing in Resource-Limited Wireless Systems

圧縮センシングの省資源無線システムへの応用に関する研究

指導教員　　**森川 博之 教授**

東京大学大学院工学系研究科
電気系工学専攻

氏　　名　**37-126519**

Theerat Sakdejayont
ティラット サクデーシャヨン

提 出 日　**2014年2月6日**

Abstract

This thesis explores the applications of compressed sensing (CS) in wireless communication contexts. CS exploits the signal sparsity to overcome resource limitation in wireless systems. This thesis considers two scenarios: wireless sensor network and wideband wireless communication.

Wireless sensor networks generate big-data which lead to overwhelming traffic in the networks. In order to reduce traffic, we apply 1-bit CS with a structured measurement matrix to suit with wireless sensor data and memory limitation of sensor nodes. The evaluation on sensor data and the implementation on sensor nodes validate the viability on a practical system.

Wideband wireless communications require high-speed ADCs to sample wideband signals due to the Nyquist theorem. Sub-Nyquist sampling relaxes the requirement by exploiting CS theory. Narrowband signals sparsely located in wideband spectrum can be sampled by two CS-based sub-Nyquist sampling systems: Random Demodulation based system and Modulated Wideband Converter. The simulation and the implementation shows the performance of the sub-Nyquist sampling systems in various scenarios.

Contents

List of Figures

List of Tables

Chapter 1

Introduction

> "Why go to so much effort to acquire **all** the data when **most** of what we get will be thrown away? Can we not just **directly measure** the part that will not end up being thrown away?"
>
> (*David L. Donoho*)

Compressed sensing (CS) [3] is another buzzword of a signal processing technique which has a potential in many application fields. What CS attempts is intuitively explained by the above quotation. The basic principle of applying CS is to sample a signal at the information rate by exploiting incoherent measurement and a sparsity of the signal, where "sparse" means when a signal can be expressed as a large number of zero or nearly zero values and a small number of non-zero values. The potential of CS has attracted abundant interest in the research community since 2006. However, limited researches have translated CS theory into practical applications, and also demonstrated an evaluation in real situations or a comparison with conventional approaches.

This thesis explores the applications of CS in resourced-limited wireless systems: wireless sensor network and wideband wireless communication.

1.1 Resourced-limited wireless systems

1.1.1 Wireless sensor networks

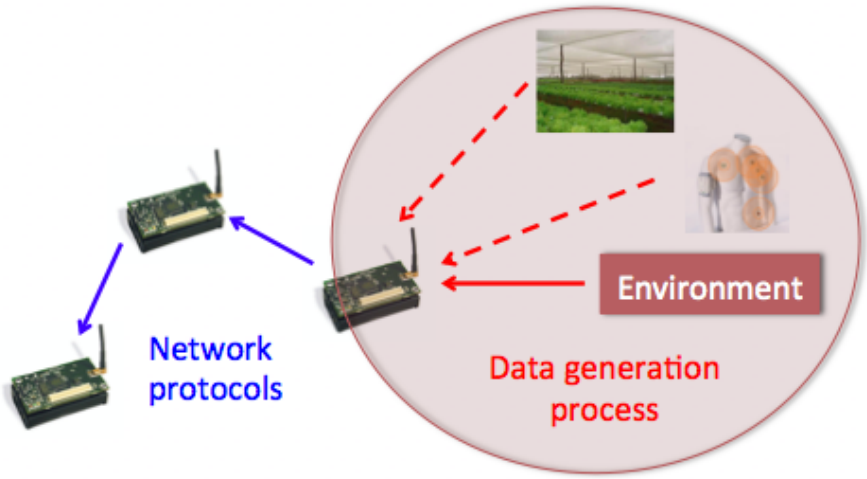

Fig. 1.1 Data generation in WSN.

Wireless sensor networks (WSN) are composed of large number of distributed-sensing nodes, which capture environment data and communicate with each other via wireless communication. The sensing nodes have a processing unit with memory to process tasks, a wireless radio unit to communicate, one or more sensors, and a power supply. Many different sensors can be used such as temperature, light intensity and humidity sensors as well as accelerometer.

Compared with traditional computer networks, WSN are usually based on small sensor nodes with limited processing power, small memory, and especially limited power supply. In a sensor node, a communication module is considered the most energy consuming part which is accounted as approximately 80%, where the rest 20% of power is consumed by sensing and processing [4].

Data compression is an option to reduce the total power consumption by reducing the power consumption of the power-hungry communication module. However, this has a trade off with the power consumption in the sensing and processing part. The data compression which is part of data generation process as shown in Fig 1.1 can be performed in order to reduce the amount of wireless traffic. The benefits of traffic reduction are as follows:

- To reduce the transmission power which is the most energy consumption part in a sensor node. This can either extend the battery maintenance period or make a sensor node sustainable by an embedded energy harvesting unit.
- To reduce the requirement of bandwidth to transfer data. An operation such as data collection and bulk data transfer requires less time and a user may obtain information more promptly.
- To relax the necessity of data storage expansion. In the future, WSNs can be densely deployed anywhere and generate tremendous amount of data which will be stored in a datacenter. The sensed data should shrink down in size while the important information is still preserved.

Although data compression provides significant improvements to WSN, the design of data compression algorithms needs to satisfy the constraints and resource limitations of WSN. The design in this thesis aims to obtain minimal error, minimal data delay, and feasibility in limited memory.

Chapter 3 describes the design of CS-based compression algorithm which suits to the WSN environment. We evaluate the algorithm with real sensor data: temperature, humidity, illuminance and implement the algorithm in off-the-shelf sensor nodes.

1.1.2 Wideband wireless communications

Wideband wireless communications refer to scenarios where a system has to sample the signal from the entire wide spectrum before extracting a informative data out of the signal in digital domain. The scenarios can be categorized as two main types:

（1） Signals sparsely located in wide spectrum. The example of this scenario is an cognitive radio system. This refers to the sparsity in the frequency domain and is based on the assumption that many wireless channels are not always occupied, according to the FCC report [1]. A frequency sparse signal can be demonstrated in Figure 1.2. In the future of wireless communication, radio devices are required to be more flexible. They may support wide range of frequency spectrum in terms of Gigahertz and operate when the carrier frequency is unknown but could lie anywhere in a wide bandwidth.

（2） Ultra-wideband (UWB) impulse signal. The example of this scenario is communication and radar by using UWB impulse radio. This refers to the sparsity in the time domain. The FCC defines UWB in terms of a transmission from an antenna for which the emitted signal bandwidth exceeds the lesser of between either 500 MHz or 20% of the center frequency and restricts the equivalent isotropically radiated power (EIRP) to be generally less that -40 dBm [5].

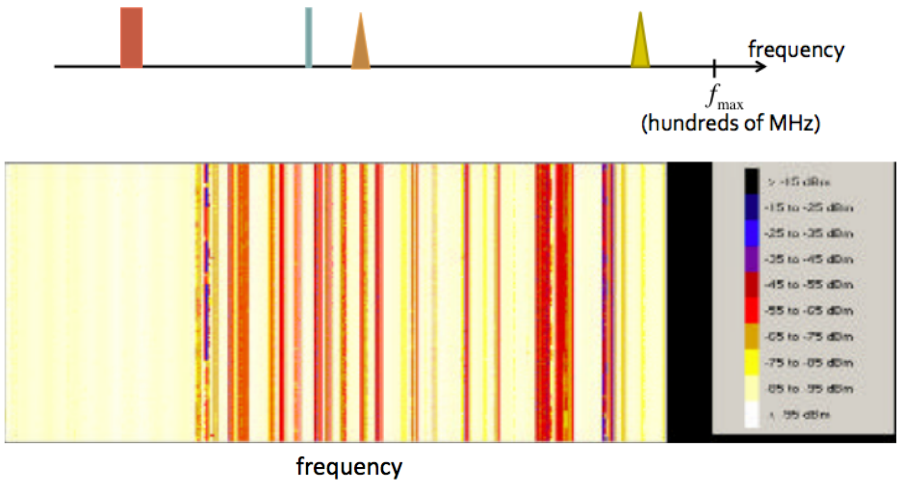

Fig. 1.2 Graphical representation of sparse frequency spectrum and its real example [1].

By basic analog-to-digital converters (ADCs), both scenarios requires a high-speed signal sampling that covers the whole wide spectrum for perfect data reconstruction. ADCs are boundary between real analog world and modern signal processing domain – discrete-time world. To deal with wideband signal where frequency tone locations are unknown in case

of (1), the sampling rate of traditional ADCs needs to be at least twice of the highest signal frequency according to the Shannon-Nyquist sampling theorem [6]. Due to the current progress of technology, high-speed ADCs are limited and may not support such future applications. Also, the current state-of-the-art ADCs operating at the order of Giga samples-per-second still consume high power and have limited bit resolution [7–9]. Hence, sub-Nyquist sampling [10], i.e. the sampling system whose sampling rate is below the Nyquist rate, attracts researchers' interest to potentially overcome the necessity of high-speed ADCs for sampling wideband signals [11–14].

This thesis focuses on the sampling of the case (1) signals sparsely located in wide spectrum. Chapter 4 describes CS-based sub-Nyquist sampling systems including Random Demodulation based system and Modulated Wideband Converter. We evaluate the performance of them by simulation based on the scenario with signals sparsely located in wide spectrum. The implementation of sub-Nyquist sampling with BPSK signals is done on laboratory-instrument level to verify the simulation results.

1.2 Thesis overview

This thesis contains four chapters. It is organized as follows:

Chapter 1: Introduction

This chapter introduces the objective of this thesis and also the motivation to apply CS for two target resource-limited wireless systems: wireless sensor networks and wideband wireless communications.

Chapter 2: Background of compressed sensing

The basic mathematical background of CS is given in this chapter. We provide some example applications of CS in addition to wireless sensor networks and wideband wireless communications. Advantages and disadvantages of CS are also discussed.

Chapter 3: CS for wireless sensor networks

In this chapter, the application of CS on wireless sensor networks is discussed. The design of CS-based data compression algorithm which suits to the WSN environment is introduced based on 1-bit compressed sensing and structured measurement matrix. The evaluation by using real sensor data and the implementation on off-the-shelf sensor nodes are also described.

Chapter 4: CS for wideband wireless communications

This chapter presents the application of CS for wideband wireless communications. CS-based sub-Nyquist sampling systems including Random Demodulation based system and Modulated Wideband Converter system are described. The performance of sub-Nyquist sampling for signals sparsely located in wide spectrum is studied by simulation and implementation.

Chapter 5: Conclusions and future works

This chapter summarizes the contributions of this thesis as well as future improvements.

Chapter 2

Background of Compressed Sensing

In this chapter, we provide basic mathematical background of CS and also several examples of applications employing CS concept. After that, we describe general advantages and disadvantages of CS,

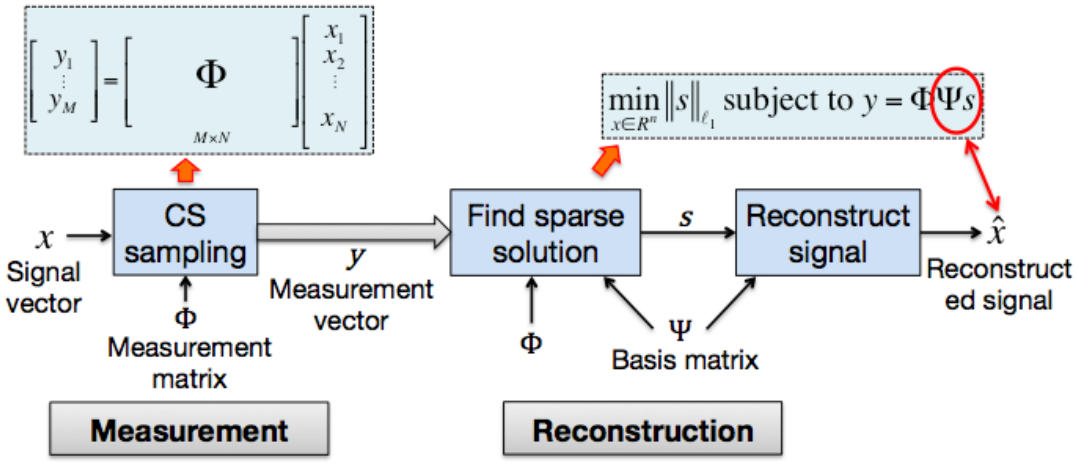

Fig. 2.1 Block diagram of compressed sensing.

2.1 Mathematical background

When the original signals can be expressed as a large number of zero or nearly zero values and a small number of non-zero values, the signals are said to be sparse or compressible. CS is a state-of-the-art data acquisition theory that exploits the incoherent measurement and the fact that many natural signals are sparse or compressible in the appropriate basis such as Fourier transform, Discrete Cosine Transform (DCT), and Discrete Wavelet Transform(DWT) etc. [3,15]. CS typical represents signals in terms of discrete-time matrix form.

Figure 2.1 shows the block diagram of CS. CS sampling is performed in analog front end in our consideration. A measurement vector $\mathbf{y}$ which is an outcome of CS sampling is passed to a reconstruction process. The reconstruction firstly find a sparse solution $\mathbf{s}$ according to $l1$-norm minimization problem and then transform the sparse solution to a reconstructed signal corresponding to a sparsifying basis.

Mathematically, let an $N \times 1$ signal vector $\mathbf{x}$ can be represented as an $N \times 1$ sparse vector $\mathbf{s}$ with the relationship

$$\mathbf{x} = \mathbf{\Psi s}, \tag{2.1}$$

where $\mathbf{\Psi}$ is an $N \times N$ basis matrix. In the CS sampling, the original signal vector $\mathbf{x}$ is compressed by an $M \times N$ measurement matrix $\mathbf{\Phi}$ as follows

$$\mathbf{y} = \mathbf{\Phi x} = \mathbf{\Phi \Psi s}, \tag{2.2}$$

where $\mathbf{y}$ denotes the $M \times 1$ acquired CS measurement vector. The measurement matrix $\mathbf{\Phi}$ should be incoherent with the basis $\mathbf{\Psi}$ in order to successfully reconstruct a sparse solution. To guarantee the robust and the efficient recovery of the sparse signal $\mathbf{s}$, the measurement matrix $\mathbf{\Phi}$ must obey the "restricted isometry property (RIP)" [16]

$$(1-\delta)\left\|\mathbf{s}\right\|_2^2 \leq \left\|\mathbf{\Phi \Psi s}\right\| \leq (1+\delta)\left\|\mathbf{s}\right\|_2^2, \tag{2.3}$$

where $\left\|\mathbf{s}\right\|_2^2 = \sum_i {s_i}^2$ and $\delta(0 \leq \delta < 1)$ is the smallest isometry constant that satisfies Eq. (2.3). This property is difficult to verify. Practically, it is required that coherence between the measurement matrix $\mathbf{\Phi}$ and the basis $\mathbf{\Psi}$ is small enough. To define the degree of compression, the compression ratio is defined as

$$\text{compression ratio} = \frac{\text{compressed size}}{\text{original size}} \times 100\%. \tag{2.4}$$

CS framework recovers a sparse vector $\mathbf{s}$ from only these linear measurements with the knowledge of $\mathbf{\Phi}$ and $\mathbf{\Psi}$ at the reconstruction. Typically, the inverse problem of Eq. (2.2) is an ill-posed problem that generally cannot be uniquely solved. However, under the assumption that the signal vector $\mathbf{x}$ can be expressed in the basis $\mathbf{\Psi}$, $\mathbf{s}$ can be estimated by solving the following $l1$ norm minimization

$$\min \left\|\mathbf{s}\right\|_1 \text{ subject to } \mathbf{y} = \mathbf{\Phi \Psi s}, \tag{2.5}$$

where $\left\|\mathbf{s}\right\|_1 = \sum_i |s_i|$. If the RIP is satisfied, the sparse solution $\mathbf{s}$ can be successfully reconstructed with high probability. Nevertheless, in the real world a signal is not perfectly K-sparse where instead of exactly K entries are non-zero values, K entries have relatively high value compared to the other almost zero or zero entries.

Eq. (2.5) can be solved by several reconstruction algorithms categorized as three main types: convex optimization algorithms [17, 18], combinatorial algorithms [19], and greedy algorithms [20,21]. Greedy algorithms provide a compromise between convex optimization algorithms and combinatorial algorithms in terms of the required number of measurements

and computational complexity, where convex optimization algorithms require least number of measurements but incur most expensive computation.

Traditionally, one would collect data samples as $\mathbf{x}$ by using ADCs and then compress it using matrix multiplication where this method is so called "digital CS". On the other hand, CS offers an impressive alternative by collecting roughly M samples using simple analog measurement, thus sampling and compressing at the same time. This method which can be categorized as "analog CS". Since the compression occurs in the analog sensor read-out electronics prior to ADCs, the analog CS can eliminate the necessity of the high-speed ADC.

2.2 Applications

> "Many natural signals are sparse or compressible in the sense that they have concise representations when expressed in the proper basis."
>
> (*Emmanuel J. Candès*)

As inspired by one of the pioneers of CS, many applications adopting CS concept have emerged. Since this thesis considers only two applications of CS, we here show some examples of them.

- Optical imaging. One of the most well-known CS devices is "single-pixel camera" developed by Rice University [22]. The idea is to trade spatial resolution for temporal resolution. The camera uses a single pixel to capture many measurements over time. Each measurement encodes the light information from the entire scene by using a micro-mirror array which is a grid of pixel-like mirrors. An individual pixel-like mirror may reflect the light either toward the single-pixel light sensor or to some other directions. The mechanism can be modelled as a binary measurement matrix.
- Medical Resonance Imaging (MRI). MRI is a promising application of CS. Applying CS to MRI allows the reconstruction possible with fewer samples than conventionally needed [23]. Fewer samples means faster scans so patients can spend less time staying static during the examination.
- Seismic imaging. Seismic imaging has utilized the sparse approximation and CS-based seismic imaging system can be done by manipulating the excitation signal e.g. one sent by a ship and controlled explosion [24]. Another method is done in

the receiving scheme where the rate and location of samples are random to obtain incoherent measurements.

- Radar. A pure CS radar refers to a design of CS-based emitter and receiver devices. The special radar pulse is designed to exploit CS and provides better resolution that traditional radars [25].
- Data coding. CS-based data coding can compress the data at high degree of compression and in real time, as a trade off with time and power consuming reconstruction. This suits to the situation with limited transmission bandwidth and low-powered sensors such as in astronomy [26]. We apply similar concept to wireless sensor networks as explained in Chapter 3.
- Analog-to-digital converter (ADC). CS can be adopted in sampling system to brake the link between the sampling speed and the signal bandwidth. CS-based sampling systems, which can acquire a signal according to its amount of information, are discussed in Chapter 4.

2.3 Advantages and disadvantages

CS has its own characteristics that determines whether it suits to a target application. The advantages of CS include simplicity of the measurement process, flexibility, and generality. However, it also has some drawbacks including complexity of the reconstruction process, and sensitivity to noise.

To begin with, one of the major advantages of CS is that it trades a processing load from data acquisition part to data reconstruction process. This provides the simplicity in the measurement process which is modelled as a linear, non-adaptive matrix multiplication. This property is preferred by most of applications in which the signal acquisition is troublesome and critical, e.g. when the computational resources, the acquisition time, or the sensor hardware are limited. In this kind of applications, CS can provide a saving in terms of size, weight, power, or costs of acquisition devices.

Another main advantage of CS is its universality. In most applications, the same random measurement matrix can be used for all signals. Typically, the measurement matrix that is designed as an arbitrary random matrix satisfies CS theory because the measurement matrix is usually incoherent with most fixed transformation basis. The application such described in Chapter 3 utilizes this property.

Moreover, flexibility is another merit. CS sampling does not have to know what basis the signal is sparse in. The sparsifying basis can be freely chosen at the reconstruction process. This implies that we can improve the accuracy of the reconstruction over time by obtaining more-sparse representation as long as a new sparsifying basis is incoherent with the measurement, even though the samples have been measured in the past.

On the other hand, a major disadvantage of CS is the reconstruction complexity. The post-process of the measurements is a time consuming process to recovery the signal. The computation complexity is in terms of polynomial time. Since the load has been reduced in the measurement side, the reconstruction generally requires more processing time and higher computational capacity done by powerful or specifically designed processing units.

Also, CS is sensitive to input noise. Due to the incoherent measurement, the information including noise are spread through out the measurements. The measurement process aliases all the noise in the signal into the compressed measurements, where this mechanism is so called “noise folding”. It reduces signal-to-noise ratio compared to that of the original signal.

In summary, due to these merits and demerits, CS may match to some applications but may not in some other cases. Even if we can utilize merits of CS to conquer a problem, there will be difficulties coming together due to its disadvantages which we require to solve.

Chapter 3

Compressed Sensing for Wireless Sensor Networks

3.1 Introduction

Compressed sensing (CS) exploits signal sparsity to reduce the amount of traffic generated from a big-data technology e.g., wireless sensor networks (WSNs) for environmental monitoring. The sensor data representing natural phenomena usually exhibits correlation among data which can be represented as sparse data in some domain. Lower power consumption for data transmission and server storage memory can be expected by applying CS-based data compression [27]. 1-bit CS can improve the performance of traffic reduction in wireless sensor networks while applying a circulant random bipolar measurement addresses the limitation of memory in sensor nodes.

CS conventionally represents high-dimensional signals in the form of smaller number of measurements by using randomized, linear, non-adaptive measurements. The conventional CS assumes that the measurements are real valued and have infinite bit precision. However, in practice the measurements are quantized into finite number of bits. In an extreme case, Boufounos et al. introduced "1-bit CS" which uses only 1-bit quantization representing sign of the measurements [28]. Although more measurements are necessary in 1-bit CS, it can finally decrease the number of bits from the original high resolution quantized bitstream.

The small sensor nodes of WSN usually have limited processing power, limited energy, and scarce memory. This work focuses on applying CS without violating the memory limitation which is crucial because it determines the feasibility of a desired application. A measurement matrix used in CS measurement is stored in sensor nodes' limited memory, and it is accounted as main memory space consumption of CS data processing algorithm. Since 1-bit CS requires more measurements which result in larger memory consumed by a measurement matrix, a circulant structured matrix [29] with entries randomly generated by Bernoulli distribution is introduced to cope with the memory issue.

In this chapter we evaluate the performance of memory-efficient 1-bit CS which adopts a circulant random bipolar measurement matrix by using real sensor data including temperature, relative humidity, and illuminance. The results show that the proposed scheme can reduce the traffic and save significant amount of memory compared to the conventional CS under same conditions. Furthermore, the experiment on real sensor nodes is also conducted to verify our scheme.

3.2 Related works

CS has been applied to WSNs in various schemes to handle the sparsity in most natural phenomena. Plenty of works [30–34] have applied similar CS-based data compression in time axis to biological signals, such as electrocardiography (ECG), electroencephalography (EEG), and electromyography (EMG) signals, gathered by body monitoring systems. In particular, [32] analyzes both analog and digital implementations in circuit models and presents in terms of EEG signals, whereas this thesis applies the digital calculation in sensor nodes' micro controller unit on environmental monitoring data. In addition, we provide a few more examples of CS-based WSN data collection protocols and a design of circuit to perform CS sampling in wireless sensor nodes. Lastly, we discuss advantages of CS to WSN in general.

CS-based data collection schemes in WSNs has been introduced by the authors of [35,36]. They share common characteristic of taking CS sampling among sensor nodes i.e. exploiting spatial correlation to compress the data, but they differ in the approaches to perform matrix multiplication of CS sampling. [35] considers rather old-fashion analog amplitude modulation and coherent transmission to achieve constructive summation in air interface in order to perform CS sampling from multiple child nodes concurrently. On the other hand, the spanning tree topology of WSN is considered in [36] and CS sampling is gradually achieved when the transmitted data is collected from child nodes to a root node. That is, a node projects its sensor data to CS measurements which is forwarded to its parent, then the parent repeats the projection and sums to the intermediate CS measurements until CS measurements reach the root node. Although this scheme reduces the transmission by nodes near the root node significantly, it increases unnecessary transmission to a leaf-node which usually send only a piece of data (its own sensor data). The problem is solved by a hybrid CS scheme [37], where if a node sends less than a number of CS measurements by the conventional method, the conventional method is used. Moreover, [38] considers the use of *sparse* random measurement matrix in the data collection of WSN. Instead of getting the measurements from all nodes, some of nodes are randomly chosen to transmit. These schemes require a spanning-tree routing algorithm which may be not the case in some network protocols [39].

Generally, CS has several merits which make it potentially suitable for WSNs. The encoding part of CS which will be performed at data sources is designed to be simple, linear, and non-adaptive. The only thing that the sensor nodes are required to perform is

matrix multiplication, whose result can gradually build up while a sample data is sensed from a sensor. Unlike thresholding-based transformation compressions which also exploit the signal sparsity in some domains by extracting high coefficients as an output, the encoding part of CS is universal among sensor data. The same encoding process with random measurement can be done even when different sensor data are sparse in different domains. The sensor nodes do not require a knowledge of which domain the data is sparse. In another aspect, the reconstruction performance of CS is improvable ceaselessly. Given CS measurements stored in a server, the discovery of better sparsifying basis for the data can be applied at the reconstruction process to improve the reconstruction performance.

3.3 Data compression for WSNs

As shown in Fig. 3.1, CS measurement is performed in data sources which is sensor nodes in our consideration. A measurement vector $\mathbf{y}$ which is an outcome of CS measurement is transmitted along the network to a root node to reconstruct the original signal. The root node which is usually a relatively high performance computer firstly finds a sparse solution $\mathbf{s}$ according to $l1$-norm minimization problem and then transform the sparse solution to a reconstructed signal corresponding to a sparsifying basis.

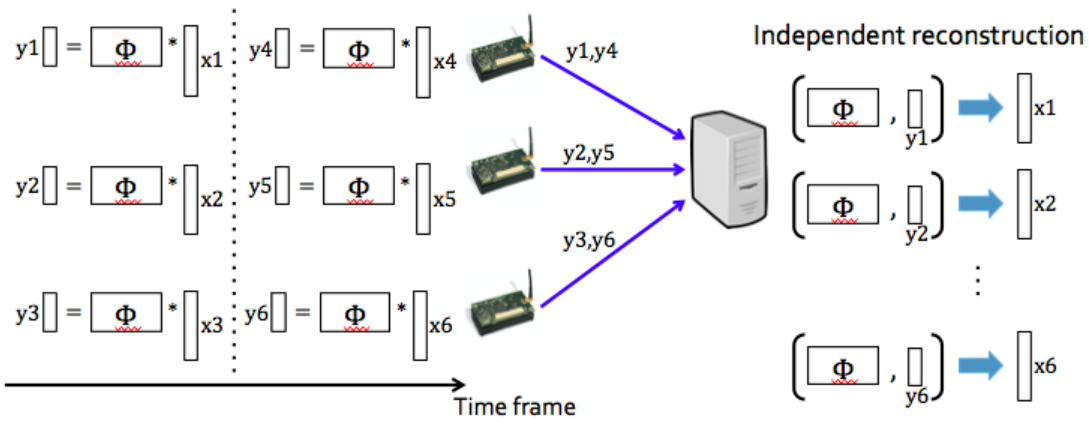

Fig. 3.1 CS sampling and reconstruction in WSNs.

3.3.1 1-bit compressed sensing

When reducing traffic at high rate, the conventional CS suffers from insufficient measurements and results in high distortion from reconstruction. Therefore, we are interested

in 1-bit CS where each measurement is quantized into one bit of sign information. At a given target number of bits of compressed data, 1-bit CS can increase the number of measurement. Despite of low resolution quantization, the additional measurements which may even exceed the number of original signal can improve the reconstruction accuracy and therefore lower distortion by 1-bit CS can be expected.

Let a length-N signal vector $\mathbf{x}$ be represented as a sparse vector $\mathbf{s}$ with the relationship $\mathbf{x} = \mathbf{\Psi s}$ where $\mathbf{\Psi}$ is a basis matrix. In 1-bit CS measurement, the original signal vector $\mathbf{x}$ is compressed by an measurement matrix $\mathbf{\Phi}$ as follows

$$\mathbf{y} = \text{sign}(\mathbf{\Phi x}) \tag{3.1}$$

where $\mathbf{y}$ denotes the length-M acquired CS measurement vector. sign() function returns 1 for positive numbers and -1 for negative numbers. Note that the conventional CS assumes that the measurements $\mathbf{y}$ are real valued and have infinite bit precision. Therefore Eq. (3.1) becomes $\mathbf{y} = \mathbf{\Phi x}$. However, in practice measurements $\mathbf{y}$ have to be quantized to a discrete value over some finite range before being further processed. Let a system quantization be B bits. A total compression rate including quantization R_c is defined as the ratio between the number of bits required for a compressed and an original signal such that $R_c = M_{conv}/N$ for the conventional CS and $R_c = M_{1bit}/BN$ for 1-bit CS.

Although the amplitude information is lost during 1-bit measurement stage, the reconstruction method [28] was proposed to enforce that the sparse solution $\mathbf{s}$ lies on the unit sphere and the $l1$ norm minimization problem becomes

$$\min \|\mathbf{s}\|_1 \text{ subject to } \mathbf{y} = \text{sign}(\mathbf{\Phi\Psi s}), \|\mathbf{s}\|_2 = 1. \tag{3.2}$$

As a comparison between the conventional and 1-bit CS, 1-bit CS can increase the number of measurement to BR_cN compared to that of the conventional CS at R_cN at a given target number of bits of compressed data. However, due to larger measurement matrix, memory requirement of 1-bit CS are increased by a factor of B to store the larger measurement matrix.

3.3.2 Structured measurement matrix

Generally, we require that coherence between the measurement matrix $\mathbf{\Phi}$ and the basis $\mathbf{\Psi}$ is small enough. A good choice for the measurement matrix $\mathbf{\Phi}$ is random matrices. In this work we consider two classes of sub-Gaussian distribution measurement matrix, namely Gaussian and bipolar random matrix. Since entries in bipolar random matrix are only 1 and -1 which can be represented by only 1 bit, the use of bipolar random matrix as a measurement matrix can save some memory.

Instead of storing the fully random measurement matrix which occupies large memory space, applying partial random structured matrices as measurement matrices is encouraged. It has been shown that circulant random matrices with entries generated independently from the same distributions are also sufficient to satisfy the RIP (restricted isometry geometry) with high probability [40]. Given a stem vector $\mathbf{c} = (c_0, ..., c_i)^T$ where $i = \max(M, N)$, the circulant matrix can be drawn as

$$\mathbf{C} = \begin{bmatrix} c_0 & c_{i-1} & \cdots & c_1 \\ c_1 & c_0 & \cdots & c_2 \\ \vdots & \vdots & & \vdots \\ c_{i-1} & c_{i-2} & \cdots & c_0 \end{bmatrix}. \tag{3.3}$$

In the conventional CS, we are interested when a number of raw signal N is larger than a number of measurement M, the measurement matrix will be a row submatrix of $\mathbf{C}$. However, in most cases of 1-bit CS, a number of measurement M grows larger than a number of raw signal N. The constructed measurement matrix will be a column submatrix of $\mathbf{C}$.

By using the circulant matrix, the memory required for storing measurement matrices is reduced significantly. The memory for storing conventional CS measurement matrices is reduced to $O(N)$, unlike fully random matrices which occupy $O(R_c N^2)$. In the $M > N$ 1-bit CS case, structured matrices consume $O(BR_cN)$ memory, while fully random matrices use $O(BR_cN^2)$. This comparison is done based on a given fixed number of target compressed bits so that we can compare between the conventional CS and 1-bit CS.

3.4 Evaluation

We evaluate the performance of 1-bit CS with circulant random bipolar measurement by using real sensor data including temperature, relative humidity, illuminance of visible light (320 nm to 730 nm). The raw data is sensed by using TelosB wireless sensor nodes [39] from a tomato greenhouse during November 24th to December 5th [41].

3.4.1 Simulation

We compare the introduced scheme with the conventional CS and a fully random Gaussian measurement, and their combinations. The conventional CS uses $B = 16$ bits for quantization. GPSR [18] and BIHT [42] are used as reconstruction algorithms for the conventional and 1-bit CS, respectively. Due to the isolation of complex numbers and the exploitation of time correlation, DCT basis is employed as our sparsifying basis. Fig. 3.2 shows the example of DCT coefficients of each data. The evaluation is done in MATLAB by using 10-day data collected from 83 sensors. The data are compressed and reconstructed independently every hour (120 samples). It is worthwhile to notice that the signal vector $\mathbf{x}$ is consistently removed the DC component, and both the DC component and the norm are used to reconstruct the absolute data.

Fig. 3.3 shows the accuracy performance in terms of average absolute error at a corresponding compression rate of all three evaluated data. The results of different kinds of sensor data all agree to the same conclusion. As mentioned in Section 3.3.1, the convention CS undergoes inadequate number of measurements that further lose more degree of freedom when using the structured matrix. As a result, applying the circulant random matrix to the conventional CS is undesirable option unlike using it with 1-bit CS. In 1-bit CS the distortion is slightly enhanced. In particularly, when the compression rate is 0.1, the distortion increased from when using fully random measurement matrix to when using circulant measurement matrix is elaborated as the following numbers: from 0.06°C to 0.08°C for temperature, from 0.18%RH to 0.24%RH for humidity, and from 11.7 lux to 12.9 lux for illuminance. Therefore, it is worthwhile to obtain significantly more compact measurement matrix.

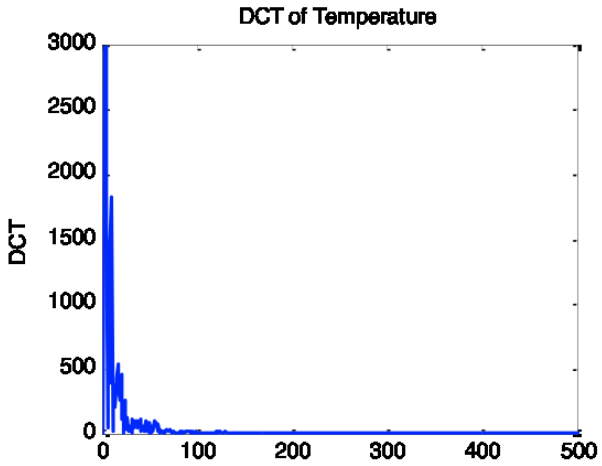

(a) Temperature

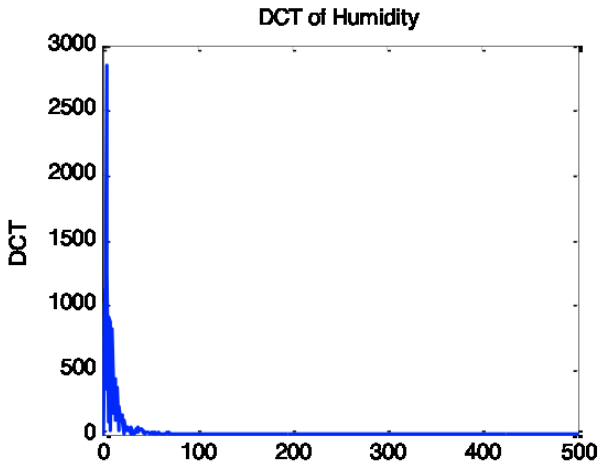

(b) Relative humidity

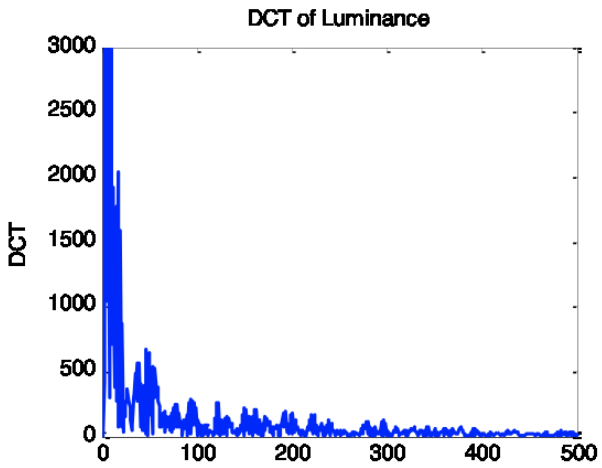

(c) Illuminance

Fig. 3.2 Example of DCT coefficients of sensor data.

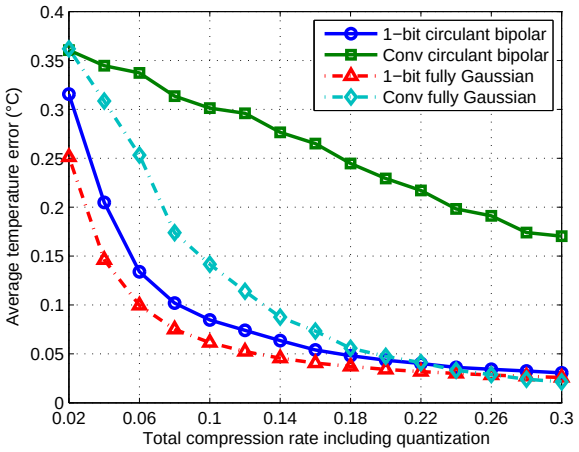

(a) Temperature

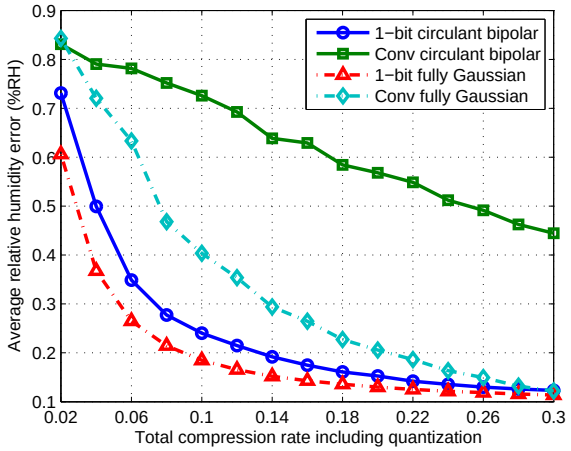

(b) Relative humidity

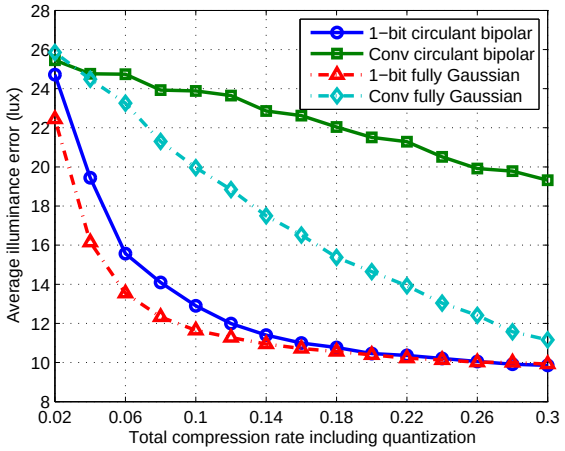

(c) Illuminance

Fig. 3.3 Average absolute error comparison in terms of compression rate.

3.4.2 Implementation

The implementation of the proposed scheme illustrates the feasibility on real sensor nodes. We implemented it on TelosB nodes whose ROM memory is 48 KB. A sensor acquires the data from an outdoor environment every 30 seconds and transmits by using reliable data collection protocol [39]. At compression rate of 0.1, the proposed scheme consumes only 24 B for storing a measurement matrix, while the fully random Gaussian measurement matrix would occupy up to 2.9 KB and 46 KB in case of the conventional and 1-bit CS, respectively. Fig. 3.4 shows an example of 1-day data with its reconstruction. The maximum absolute errors of each sensor data are 0.37°C, 0.42%RH, and 79 lux for temperature, humidity, and illuminance, respectively. In short, the scheme decreases 90% of traffic without significant effect on memory consumption and accuracy.

In this chapter, we have evaluated the reconstruction accuracy in terms of distortion which is measured in absolute difference in real world unit because it can give an idea on real application and also be comparable to a sensor performance. The TelosB wireless sensor nodes are equipped with an SHT11 humidity and temperature sensor. The SHT11's temperature sensing can provide ±0.5°C at 25°C accuracy with ±0.1°C repeatability, and the accuracy of ±3.5%RH along with the repeatability of ±0.1%RH for the relative humidity. The results show that the CS-based compression and reconstruction can achieve the same order of error with the sensor performance. The reconstruction of temperature and relative humidity data are considerably accurate enough for most monitoring applications. On the other hand, the fluctuating illuminance data cannot be recovered precisely at the abrupt peak. The sharp peak results in low sparsity in DCT domain, and therefore the illuminance data has least degree of compressibility compared to other two data.

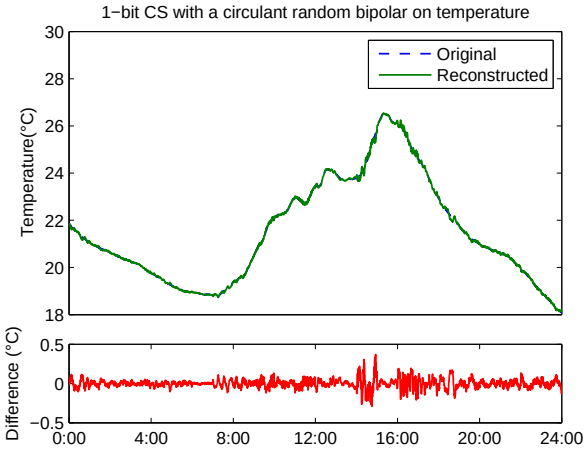

(a) Temperature

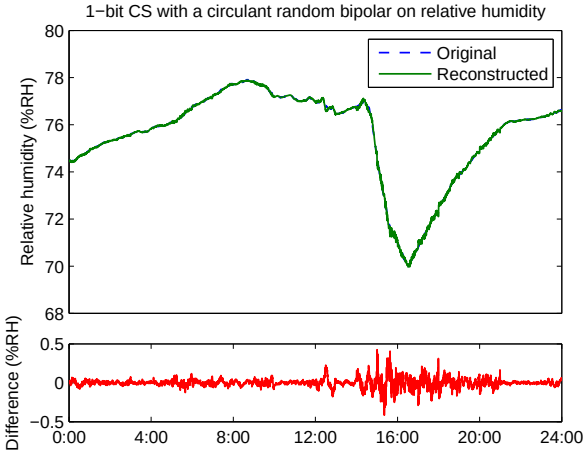

(b) Relative humidity

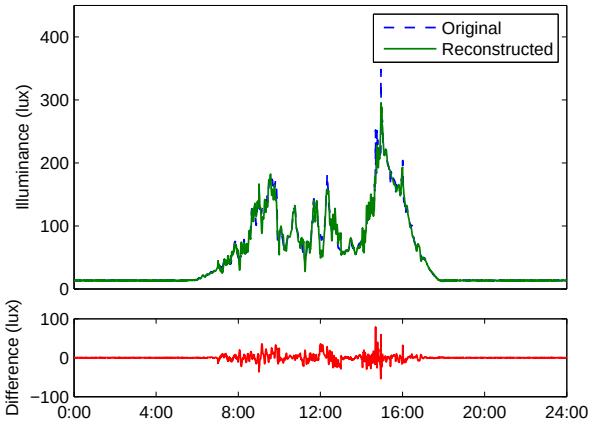

(c) Illuminance

Fig. 3.4 Example of 1-day data and its reconstruction.

Table. 3.1 Comparison of CS measurement schemes.

Metric	Conv. CS (B-bit CS)		1-bit CS	
	Fully rand.	Part. rand.	Fully rand.	Part. rand.
Distortion: high R_c	Very low	High	Low	Low
Distortion: low R_c	Very high	Very high	Moderate	High
Memory	$O(R_cN^2)$	$O(N)$	$O(BR_cN^2)$	$O(BR_cN)$

Note that B represents bit resolution and a compression rate R_c is defined the ratio between the number of bits required for a compressed and an original signal.

Finally, Table 3.1 summarizes the characteristics of the conventional CS and 1-bit CS with different measurement matrices according to the calculation in Section 3.3.2 and the evaluation in Section 3.4. Notably, 1-bit CS with the structured measurement matrix achieves memory-efficient with sufficiently low distortion which suits to memory-limited applications employing small sensor nodes.

As a remark for other applications for monitoring with different constraints, we provide some suggestions based on our results. Without the memory limitation, the conventional CS with fully random measurement matrix can provide very low distortion at considerably good compression ratio and therefore is a good choice for high accuracy applications, while 1-bit CS with fully random matrix can highly compress the data so that it is suitable to transmission expensive applications such as satellite remote monitoring applications.

3.5 Summary

This chapter shows an empirical study of 1-bit compressed sensing with a circulant random bipolar measurement on real sensor data which consists of temperature, relative humidity, and illuminance. The evaluation results demonstrate that in case of resource-limited wireless sensor networks, one may consider the circulant bipolar measurement matrix operating in 1-bit compressed sensing scheme as an outstanding candidate. The implementation on real sensor nodes also reveals the feasibility of the introduced scheme practically.

Chapter 4

Compressed Sensing for Wideband Communications

4.1 Introduction

High-speed ADCs are necessary to sample wideband signals due to the Nyquist theorem. However, high-speed ADCs operating at the level of tens of gigasample-per-second are still impractical by current technology [7–9]. Sub-Nyquist sampling relaxes the requirement of Shannon-Nyquist theorem, i.e. reduces a sampling rate below the Nyquist rate, by exploiting the sparsity of wideband signals along with CS theory. Instead of using a high-speed ADC, a wideband signal can be acquired by using low-speed ADCs with the signal preconditioning i.e. analog compressed sensing.

In this thesis, we consider a wideband signal whose spectrum is sparse. Within wideband spectrum, there are narrowband signals existing in the sparse fashion. This is under the assumption that most part of the bandwidth is not always occupied simultaneously [1]. A possible application of sub-Nyquist sampling could be cognitive radio system, where the sampling circuit of devices has to acquire the entire wide frequency band without carrier demodulation due to the lack of prior knowledge of carrier frequency before the sampling.

This chapter describes CS-based sub-Nyquist sampling including two systems: Random Demodulation (RD) based system [11, 14] and Modulated Wideband Converter (MWC) [43]. RD-based system is based on signals in finite discrete model which discretizes the frequency spectrum in discrete manner i.e. signals are traditionally viewed as a summation of sinusoidal wave with discrete frequency. On the other hand, MWC system is based on signals in infinite continuous model. MWC system can sample a band-limited signal from wideband spectrum with low reconstruction complexity.

Previous works have mainly focused on the theoretical proof of concept in ideal situations [12, 14, 43] and their prototype circuit design [44, 13, 45–47], but the performance of a sub-Nyquist sampling system in more practical situation has not been discussed intensively. The contribution of this thesis on either systems is described separately as follows:

- In RD-based system, we consider the mixing process where the selection of chipping frequency of PN sequences is essential and still remains unexplored. The effect of the chipping frequency variation is studied along with hardware nonidealities including circuit noise, clock jitter and rise/fall of PN sequences.
- In MWC system, the evaluation is done in terms of digital communication - bit error rate (BER) of BPSK/QPSK modulated signals, and thus the comparison between the traditional Nyquist sampling is achieved. The effect of the chipping frequency

variation is also studied. The implementation on laboratory-instrument is done level to verify the simulation results.

4.2 Related works

In order to obtain effective high-speed sampling, although a Nyquist-rate time-interleaved system [48] can combine n f_{ADC}-sample-per-second ADCs to act as an nf_{ADC}-sample-per-second ADC, many researches have been done to exploit a prior knowledge to achieve a sub-Nyquist system.

Dating back to the history, non-CS sub-Nyquist sampling systems have existed, but due to hardware limitation some of them are not implemented commercially [49, 50]. The traditional sub-Nyquist sampling system with a prior knowledge of a band location is demodulation (also known as down shifting). This scheme has been used widely in current radio systems. A tunable local oscillator is dedicated to acquire one signal band. If the information exist in multiple bands, then one has to redesign the analog hardware according to the number of bands. Direct bandpass sampling [49] simply samples the signal at sub-Nyquist rate which causes aliasing. [49] derives conditions to successfully acquire beneficial aliasing. However, the conditions are difficult to be satisfied in practice. Also, although a low-speed ADC can be applied, it still needs to support high analog bandwidth according to the maximum frequency of the signal. Another sub-Nyquist sampling system is periodic nonuniform sampling [50], which is actually a subsystem of time-interleaved ADC system. This concept also exploits signal sparsity like CS, but frequency support is known priori. Due to the direct point-wise sampling of input signal, high analog bandwidth of ADCs is still required.

Since the emergence of CS plenty of researches have attempted to apply the concept to sub-Nyquist sampling systems. In CS-based systems, instead of high sampling speed of ADCs, there must be another components operating at high speed or bandwidth. Both fully random sampling [51] and multicoset sampling [52] requires Nyquist-rate bandwidth of ADCs, while [53] and [54], which perform random filtering and filter bank respectively, also requires Nyquist-rate bandwidth of filter in addition to the ADCs. Two similar promising architectures are RD [11] and MWC [43] that utilize naturally supporting high-bandwidth devices like mixers and high-speed sequence generators. Though both of them are similar in measurement circuit, the reconstruction behind are difference as discussed later in Section 4.3. RD-based sub-Nyquist sampling theories have existed in the literature

for many years. This system architecture is originated from [55, 11] and developed more detailed explanation in [12]. The extension to multiple signal paths is developed by Yu et al. [13]. Its modified version also supports an input signal which is sparse in time-frequency domain such as in short-pulse radar application [56]. The prototype circuit implementation can be found in [44, 13, 45, 46]. On the other hand, MWC [43, 47] was firstly introduced in recent few years with fully theoretical explanation and proof-of-concept implementation. However, to the best of our knowledge, none of previous works has not considered the effect of PN chipping frequency and intensive BER evaluation of MWC which will be considered in this chapter.

4.3 Sub-Nyquist sampling

A signal sparsely located in wideband spectrum can be sampled at sub-Nyquist rate by two main systems: Random Demodulator based system in Section 4.3.1 and Modulated Wideband Converter in Section 4.3.2. In each section, system model and its overclocked version are explained.

4.3.1 Random Demodulation based system

(a) System model

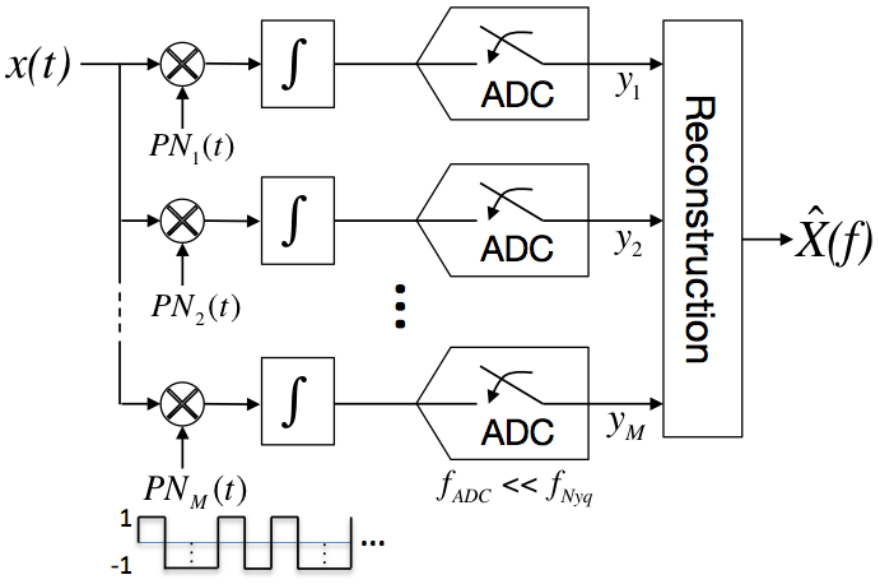

Fig. 4.1 Block diagram of RD-based sub-Nyquist sampling.

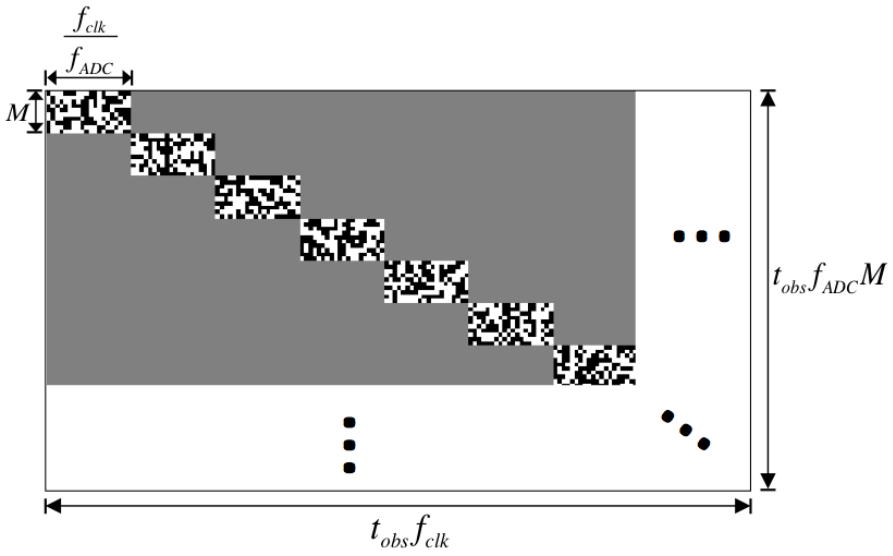

Fig. 4.2 Modeled measurement matrix of multiple-channel RD. (black: -1, white: 1, grey: 0).

The block diagram of RD-based sub-Nyquist sampling system is shown in Fig. 4.1. The analog input signal $x(t)$ is mixed with a PN sequence waveform by obtaining multiplication between them. The mixed signal is then passed to an integrate-and-dump whose output is sampled by a low-speed ADC. After that, the sampled signal is processed in the digital domain to reconstruct the signal. In the reconstruction, a sparse solution $s(f)$ is determined according to l1-norm minimization problem and then it is transformed to obtain a reconstructed original signal $x(t)$ by using invert Fourier transform. In the multiple channel architecture as presented in [14, 45], a measurement matrix considered the reconstruction process can be visualized as shown Fig. 4.2. Note that the black and white pixels represent -1 and 1 values of the PN sequence, respectively, whereas the grey area is 0.

Let us present a mathematical model of the analog signal and also the system basically in terms of one parallel channel [12]. The analog input signal $x(t)$ is K-sparse multitone signal in which there are K number of active tones during the observation time t_{obs}. The input signal $x(t)$ can be written as

$$x(t) = \sum_{f \in F} a_f e^{-j2\pi ft} \text{ for } t \in [0, t_{obs}) \tag{4.1}$$

where a_f is an amplitude of each sinusoidal component. F is a set of K frequency tone which satisfies $\Omega \subset \{0, \Delta, 2\Delta, ..., f_{max}\}$. f_{max} is the highest frequency component existing in the analog signal where each possible frequency component is equally spaced by Δ.

The PN sequence waveform that is multiplied to the input signal $x(t)$ is produced from a discrete-time chipping sequence $\varepsilon_0, \varepsilon_1, \varepsilon_2, ...$ of numbers whose values are 1 or -1. The continuous-time PN sequence waveform is created the discrete-time chipping sequence by

$$PN(t) = \varepsilon_n p(t),\ t \in \left[\frac{n}{f_{clk}}, \frac{n+1}{f_{clk}}\right), \tag{4.2}$$

where $p(t)$ is a pulse of PN sequence waveform. In ideal case, $p(t)$ is a square pulse shape represented by

$$p(t) = \begin{cases} 1 & , t \in [0, \frac{1}{f_{clk}}] \\ 0 & , \text{otherwise} \end{cases} \tag{4.3}$$

.

The result of multiplication between the input signal $x(t)$ and the PN sequence waveform $PN(t)$ is

$$y(t) = x(t) \cdot PN(t),\ t \in [0, t_{obs}). \tag{4.4}$$

. The demodulated signal $y(t)$ is passed through low-pass filter where here is simply an integrate-and-dump every $\frac{1}{f_{ADC}}$ seconds. The accumulated signal is sampled right before resetting to obtain a sequence y_m of measurements which form $\mathbf{y}$ as written by

$$y_m = f_{ADC} \int_{m/f_{ADC}}^{(m+1)/f_{ADC}} y(t)\mathrm{d}t. \tag{4.5}$$

where f_{ADC} is the sampling rate of a low-speed ADC.

Next, the measurements $\mathbf{y}$ is used to reconstruct the frequency-sparse solution $\mathbf{s}$ as described in Section 2.1. Note that since in this system we map a continuous signal to a discrete-time signal to represent in a matrix form, the reconstructed time signal $\mathbf{x}$ is discrete-time signal where its value x'_n is determined by the pulse shape of PN sequence waveform. In the ideal square pulse case, it denotes the average value of the input signal $x(t)$ over a time interval of length $1/f_{clk}$ starting from a time instant $t_n = n/f_{clk}$ for an integer n as

$$x'_n = \int_{t_n}^{t_n + 1/f_{clk}} x(t_n) p(t - t_n)\mathrm{d}t$$
$$\sum_{f \in F} s_f e^{-j2\pi f t_n} = \sum_{f \in F} a_f e^{-j2\pi f t_n} P(f).$$

Thus,

$$a_f = \frac{s_f}{P(f)} \tag{4.6}$$

where $P(f)$ is the frequency response of a pulse $p(t)$ of PN sequence waveform which is ideally the frequency response of perfect square pulse defined by

$$P(f) = \frac{e^{-j\pi \frac{f}{f_{clk}}}}{f_{clk}} \text{sinc}\left(\frac{\pi f}{f_{clk}}\right). \tag{4.7}$$

Finally, we can obtain a discrete-time representation of $x(t)$ in terms of $x[n]$ similarly to the output of a traditional uniform periodic sampling system at rate f_{clk} via the formula

$$x[n] = \sum_{f \in F} a_f e^{-j2\pi \frac{f}{f_{clk}}}. \tag{4.8}$$

(b) Overclocked system

Previous works [12, 45] usually choose the Nyquist frequency as their PN chipping frequency whose spectrum is, however, attenuated at high frequency due to their square-shaped pulse. Therefore, compensation is necessary for the proper sampling. Unfortunately, in practice the PN sequences are not perfectly square, and therefore the compensation needs troublesome calibration to determine the frequency response of an actual pulse shape. To reduce the attenuation factor within the frequency range of an input signal and consequently reduce the dependency on both compensation and calibration, we apply overclocked PN sequences to the mixing stage.

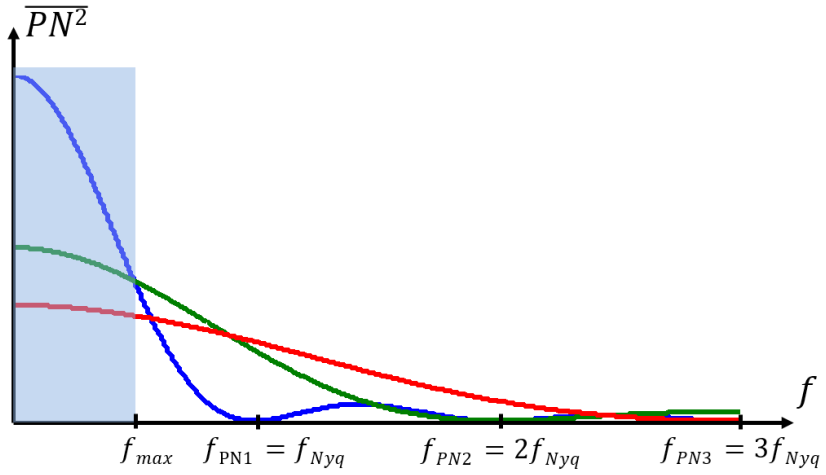

Fig. 4.3 Power spectrum of PN sequences.

In RD-based sub-Nyquist sampling, CS allows low-speed sub-Nyquist ADCs to successfully sample wideband sparse signals by mixing an input signal with minimally Nyquist-rate PN sequences. Fig. 4.3 illustrates the power spectrum of the PN sequence that

exhibits an attenuation when the frequency is increasing as described by

$$\overline{PN^2(f)} = \frac{2}{f_{clk}} \left| \text{sinc} \left(\frac{\pi f}{f_{clk}} \right) \right|^2 . \tag{4.9}$$

The existing works [14] [12] set the sequence clock frequency f_{PN} at Nyquist frequency f_{Nyq} at which the power is attenuated by 2.47 times. The extension of f_{PN} to higher frequency can flatten the power spectrum within the operating frequency band ($f < f_{max}$) as demonstrated by shaded area in Fig. 4.3.

After mixing the input signal with the PN sequence or equivalently convolution in frequency domain, the higher-frequency tones of the input signal contribute less to the mixed signal compared to lower-frequency tones. [12] compensates the attenuation in the reconstructed signal by the invert frequency response of square-shaped pulse as described in (4.7). Higher attenuation within the operative frequency band implies the more dependency to the compensation. Moreover, the PN sequences are practically not square, which usually leads to more attenuation in higher frequency. Therefore, the calibration is required to obtain a frequency response of an actual pulse shape for using in compensation step. In some systems, the calibration could be burdensome. By overclocking, the frequency spectrum becomes more level and therefore it is able to reduce the necessity of the compensation and also the calibration. Without compensation, (4.7) is approximated to $P(f) = 1$ and subsequently $a_f \approx s_f$.

As a trade-off, it can lead to higher noise vulnerability due to the reduction of overall power within the operating frequency. The power are spread to higher frequency to a flattened spectrum. The circuit noise e.g. thermal noise, quantization noise which consistently occurs inside the system may have more influence to the measurements $\mathbf{y}$.

4.3.2 Modulated Wideband Converter system

(a) System model

Fig. 4.4 shows MWC-based sub-Nyquist sampling system. Although most of the components are similar to what presented in RD-based system, the input signal and the reconstruction algorithm are difference. The input signal $x(t)$ is modeled as multiband signal in which narrowband signals existing sparsely in wide frequency band. Firstly, $x(t)$ flows into parallel channels. In each channel, $x(t)$ is mixed with the periodic PN sequence waveform whose clock rate is written as

$$f_{clk} = f_{PN} N \tag{4.10}$$

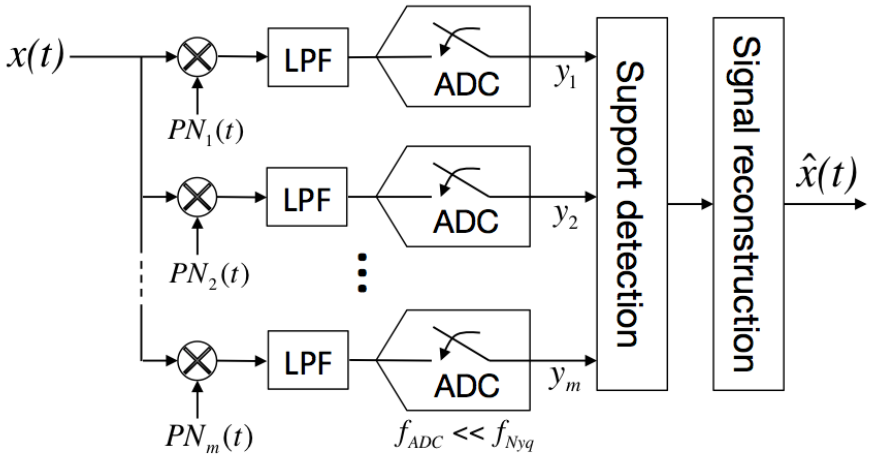

Fig. 4.4 Block diagram of MWC sub-Nyquist sampling.

where f_{PN} is the repetition frequency of the PN sequence and N is the PN code length. The mixed signal is then passed through an anti-aliasing low pass filter before being sampled by a low-speed ADC with the sampling frequency $f_{ADC} = f_{PN}$. The sampled signals from all parallel channels are fed into the reconstruction process consisting of two main steps: (1) support detection determines the band location of the signal and (2) signal reconstruction calculates the reconstructed input signal $\hat{x}$ based on the recovered support. As a necessary condition for successful reconstruction, the passband bandwidth B of the modulated signal is required to satisfy $f_{ADC} = f_{PN} \geq B$. Note that this thesis limits the consideration when $f_{ADC} = f_{PN}$ which is an option in [43], but the consideration of f_PN setting is extended later on within this section.

Let us present a mathematical model of the analog signal and also the system of MWC. The multiband input signal $x(t)$ is composed of an even number Q of bands because the conjugate symmetry in its Fourier transform is also counted. Each band occupies a bandwidth smaller than B. The bands could lie anywhere in the wide spectrum without overlapping to each other and exceeding the maximum frequency f_{max}, where the Nyquist rate of the signal is defined as $f_{Nyq} = 2f_{max}$.

Since MWC system does not rely on the square pulse shape of PN sequence waveform but only requires a periodicity, we represent the PN sequence waveform in a square pulse for simplicity. The PN sequence waveform of channel i that is multiplied to the input signal $x(t)$ is produced from a periodic discrete-time chipping sequence $\varepsilon_0, \varepsilon_1, \varepsilon_2, ..., \varepsilon_N$ of

numbers whose values are 1 or -1. It is written as

$$PN_i(t) = \varepsilon_{in}, \;\; n\frac{T_{PN}}{N} \leq t \leq (n+1)\frac{T_{PN}}{N}, \; 0 \leq n \leq N-1, \tag{4.11}$$

where $PN_i(t)$ is repeated with a period $T_{PN} = \frac{1}{f_{PN}}$ as shown in Fig. 4.5a. Due to T_{PN}-periodic, it can be written in a Fourier expansion as

$$PN_i(t) = \sum_{l=-\infty}^{\infty} c_{il} e^{j2\pi f_{PN} l t}, \tag{4.12}$$

where

$$c_{il} = \frac{1}{T_{PN}} \int_0^{T_{PN}} PN_i(t) e^{-j2\pi f_{PN} l t} dt. \tag{4.13}$$

Thus, the Fourier transform of the mixed signal $\tilde{x}_i(t) = x(t)PN_i(t)$ is

$$\tilde{X}_i(f) = \sum_{l=-\infty}^{\infty} c_{il} X(f - l f_{PN}), \tag{4.14}$$

which is a linear combination of f_{PN}-shifted copies of the Fourier transform of $x(t)$ or $X(f)$ defined as $X(f) = \int_{-\infty}^{\infty} x(t) e^{-j2\pi f t} dt$ as shown in Fig. 4.5b.

The frequency f_{PN} determines the aliasing of $X(f)$ into the spectrum of $\tilde{X}_i(f)$. The mixed signal $\tilde{x}_i(t)$ is passed through a low-pass filter and sampled by an ADC to get an informative aliased spectrum of $\tilde{X}_i(f)$. To achieve the reconstructible aliasing, the periodicity of PN sequence waveform has to be selected such that $f_{PN} \geq B$ so that at an arbitrary f_0, there are only one nonzero of $X(f_0 - l f_{PN})$ from each band where $l \in \mathbb{Z}$.

Satisfying this condition, the beneficial information for reconstructing the original signal $x(t)$ are implicitly embedded in $[-\frac{f_{PN}}{2}, \frac{f_{PN}}{2}]$, $[\frac{f_{PN}}{2}, \frac{3f_{PN}}{2}]$, $[\frac{3f_{PN}}{2}, \frac{5f_{PN}}{2}]$, etc. At least $2Q$ sets of information are theoretically necessary for signal reconstruction [43]. For example, $2Q$ sets of information can be gathered from $M = 2Q$ channels with each channel's sampling rate $f_{ADC} = f_{PN}$, or from $M = 2Q/2$ channels with each channel's sampling rate $f_{ADC} = 3f_{PN}$. In this thesis, we concentrate on when $f_{ADC} = f_{PN}$, so the cutoff frequency of the low-pass filter is $f_{ADC}/2$.

(b) Overclocked system

Since $f_{clk} = f_{PN}N$, the increase of f_{PN} can overclock the system. The overclocking of PN sequence, which is originally introduced by this work, permits the system to support wider bandwidth and therefore higher bit rate in the case of BPSK/QPSK modulated signal. In addition, the overclocking also permits untroubled higher sampling rate which eases the reconstruction and thus lower the reconstruction error, since the increase of

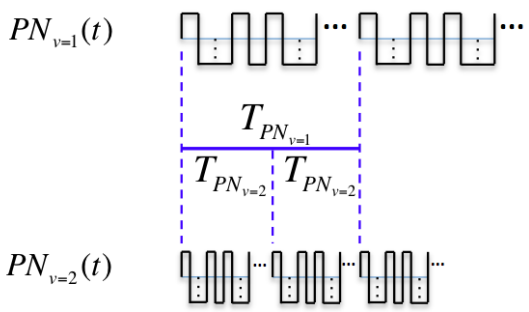

(a) Periodic PN waveform when $v = 1$ and 2.

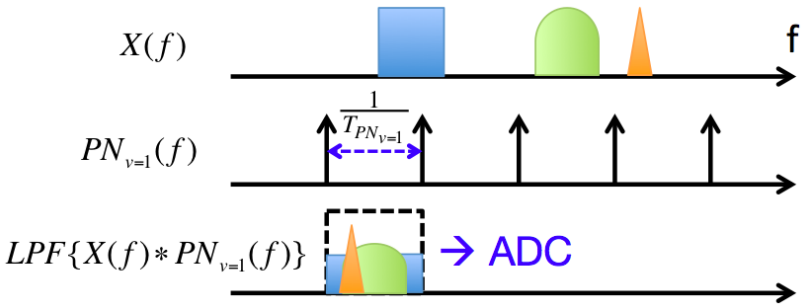

(b) Spectrum aliasing when $v = 1$.

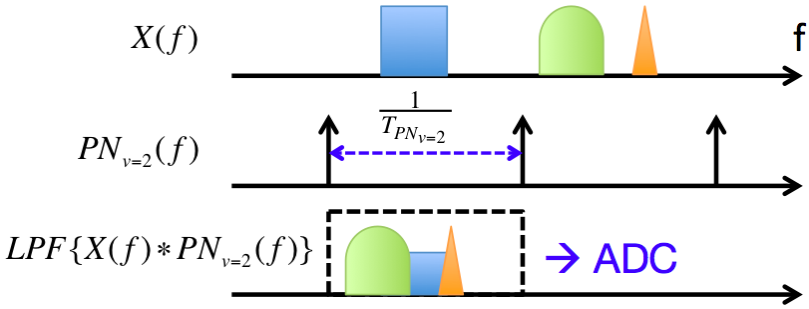

(c) Spectrum aliasing when $v = 2$.

Fig. 4.5 Periodic PN waveform and spectrum aliasing in MWC.

f_{ADC} is accordingly required to satisfy $f_{ADC} = f_{PN}$. Note that higher f_{ADC} is reasonable because it is still feasible by conventional ADC technology e.g. from 40 to 80 MHz.

Let the overclock rate be v such that $f_{PN,overclk} = v f_{PN,normalclk}$ where $v > 1$. Eq. 4.14 and 4.13 can be rewritten as

$$\tilde{X}_i(f) = \sum_{l=-\infty}^{\infty} c_{il} X(f - lvf_{PN}), \tag{4.15}$$

and

$$c_{il} = \frac{v}{T_{PN}} \int_0^{T_{PN}/v} PN_i(t) e^{-j2\pi v f_{PN} l t} dt, \tag{4.16}$$

respectively. Therefore, the sampling rate of ADC and the cutoff frequency of the low-pass filter are changed corresponding to the wider aliased spectrum as shown in Fig. 4.5c. Because the overclocking process results in the same information embedded in the sampled aliased spectrum, it provides the similar performance on support detection. However, the higher sampling rate allows better performance in signal reconstruction.

4.4 Evaluation

This section evaluates RD-based and MWC sub-Nyquist sampling systems. As shown in Table 4.1, RD-based system is designed to sample a signal modeled as a summation of finite number of sinusoidal signals, while MWC is designed to sample narrowband signal. Therefore, we evaluate them with the corresponding signals by simulation. In addition, the implementation of MWC system is discussed.

Table. 4.1 Comparison between RD-based and MWC system

Characteristics	**RD-based system**	**MWC system**
Input signal model	Sum of K sinusoidal signals	Q bands of signal, each BW $\leq B$
Reconstruction speed	Slow	Fast
Sampling delay	High	Low
Remarks	Universal but impractical amount of computation	Limited number of bands and bandwidth

4.4.1 Simulation

(a) RD-based system

In the implementation aspect, many issues have not been fully discussed in previous works. Among them, this thesis focuses on the analysis of hardware in the mixing process of RD-based systems. We consider the effect of PN chipping frequencies along with nonideal circuit parameters including circuit noise, jitter, and imperfect square pulse shape of the PN sequence.

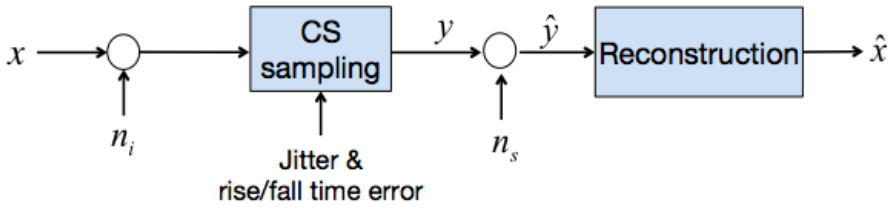

Fig. 4.6 Evaluation model of RD-based sub-Nyquist sampling.

Simulation settings

We evaluate the system over a frequency range of noise-free input signal up to the television UHF bandwidth 400 MHz. Hence, the Nyquist rate is 800 MHz. The system is simulated to sample signals from 400 subcarriers with resolution of 1 MHz. The PN sequences are generated as PRBS whose values are 1 or -1 by employing LFSR (linear-feedback shift register). Our sub-Nyquist sampling system employs 10 parallel channels (10 ADCs) where each channel is equipped with an ADC with a sampling frequency of 40 MHz. The CS reconstruction algorithm is OMP [20].

Fig. 4.6 shows the overview of this evaluation. Several practical issues are taken into accounts such as jitter and rise/fall time error of PN waveform, input noise n_i, and system noise n_s.

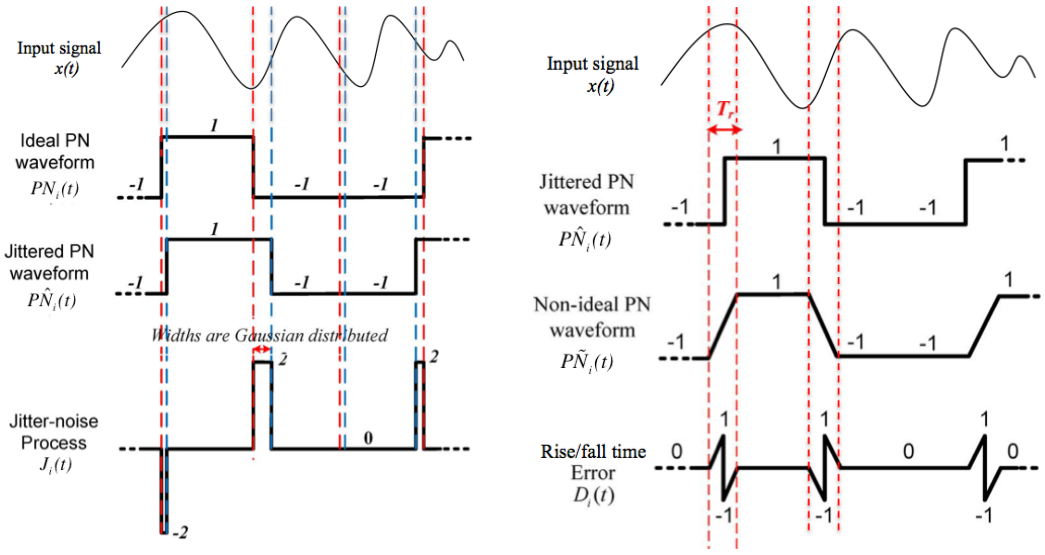

(a) Jitter error (b) Rise/fall time error

Fig. 4.7 Errors in PN sequence waveform [2].

The generation of PN sequences contains nonidealities including jitter and imperfect square pulse which affect the mixing process. The change in chipping frequency of PN sequence waveform affects the ratio of jitter noise appearing to the system, whereas imperfect square pulse requires pushes the system to be more dependent on the calibration and compensation, especially for Nyquist-rate PN chipping frequency. The modeling of jitter and rise/fall time is based on the work by Abari et al. [2].

The jitter noise is caused by the clock drift of a system clock that controls the timing in the system. Given a fixed jitter, the shorter chip interval (faster clock) enlarges the portion of the errors appearing in the PN sequence signal. The jitter noise can not be compensated after the reconstruction because of its randomness. Fig. 4.7a shows the model of jitter noise. Let a jittered PN sequence waveform denoted by $P\widehat{N}(t)$ where $P\widehat{N}(t) = PN(t) + J(t)$. The jitter noise $J(t)$ is given as

$$J(t) = \sum_j (\varepsilon_{j-1} - \varepsilon_j)\text{sign}(\varepsilon_j) p_j(t - jT_{PN}, \varepsilon_j) \tag{4.17}$$

where $p_j(t, \varepsilon_j)$ denotes a unit amplitude pulse with the pulse width equal to a jitter width ε over the interval $[\min(0, \varepsilon), \max(0, \varepsilon)]$. The jth jitter width is $\varepsilon_j \sim N(0, \sigma_J)$. σ_J which is the jitter rms is one of specifications of a clock generator. Note that all channels undergo the same jitter because the same clock generator is used.

The rise/fall time error causes the PN sequence waveform not to be perfect square-shaped pulses. It occurs due to nonidealities of circuit where a PN waveform generator takes some time to change signal's state and also a mixer does not operate instantaneously. Since these circuit nonidealities are deterministic, we can calibrate the system by the compensation after the reconstruction. However, this makes the system more dependent to the compensation and also calibration. Fig. 4.7b shows the model of rise/fall time error. Let a imperfect-square PN sequence waveform denoted by $P\widetilde{N}(t)$ where $P\widetilde{N}(t) = P\widehat{N}(t) + D(t, \varepsilon)$. Note that the reference point of the rise/fall time error is at the transition location which is dictated by the jitter noise. The rise/fall time error $D(t)$ is described as

$$D(t, \varepsilon) = \sum_j \left(\frac{\varepsilon_j - \varepsilon_{j-1}}{2} \right) q\left(t - jT_{PN} + \varepsilon_j\right) \tag{4.18}$$

where

$$q(t) = \begin{cases} \left(\frac{2t}{T_r} + 1\right) & -\frac{T_r}{2} < t \leq 0 \\ \left(\frac{2t}{T_r} - 1\right) & 0 < t < \frac{T_r}{2} \\ 0 & \text{otherwise} \end{cases} \tag{4.19}$$

where the time duration T_r defines the time required for the sequence to change its value.

When input noise n_i, and system noise n_s are considered, Eq. 2.2 can be rewritten as

$$\widehat{\mathbf{y}} = (\mathbf{\Phi x} + \mathbf{n_i}) + \mathbf{n_s}, \tag{4.20}$$

where $\mathbf{y} = (\mathbf{\Phi x} + \mathbf{n_i})$. n_i accounts for the noise of input signal at the antenna such as random disturbances in the channel, while n_s is system noise caused by CS measurement circuit. We model both of them as an i.i.d. Gaussian noise $N(0, \sigma_n)$ where the noise power P_n is σ_n^2. We quantify the amount of them as the following metrics:

$$\text{SNR of input} = \frac{\|\mathbf{x}\|_2^2}{\mathrm{E}(\|\mathbf{n_i}\|_2^2)}, \tag{4.21}$$

and

$$\text{SNR of CS measurement} = \frac{\|\mathbf{y}\|_2^2}{\mathrm{E}(\|\mathbf{n_s}\|_2^2)}. \tag{4.22}$$

Note that the SNR of input here is considered as *out-of-band* SNR, which includes the entire noise across the full bandwidth. Also, we measure the sampling performance by the accuracy of reconstructed signal defined as

$$\text{SNR of reconstruction} = \frac{\|\mathbf{x}\|_2^2}{\mathrm{E}(\|\mathbf{x} - \widehat{\mathbf{x}}\|_2^2)}, \tag{4.23}$$

where x and $\widehat{x}$ are the original and reconstructed signal, respectively. It should be noted that the original signal x is uniform periodic Nyquist-rate samples.

Simulation results

Firstly, the relationship of PN chipping frequency and sparsity rate (occupancy of frequency band) of the noiseless input signal is studied independently of other hardware nonidealities. Fig. 4.8 shows the comparison among different PN chipping frequencies in terms of SNR of the reconstruction. Fig. 4.8a and 4.8b shows the results when the compensation is applied after the reconstruction and when is not, respectively. As shown in Fig. 4.8a, since the overclocking of PN sequence widens a measurement matrix (less compression rate) modeled in the CS algorithm, the SNR of the higher PN chipping frequency starts falling earlier as the sparsity rate increases. This agrees with CS theory . When the compensation is not applied and the sparsity rate is less than 20%, higher PN chipping frequency achieves higher SNR. For example, at 10% sparsity rate, the SNR of the reconstructed signal without the compensation is increased from 1.86 dB in normal clock frequency to 13.1 dB in overclocked frequency at 3200 MHz, comparing to 56.5 dB when the compensation is applied.

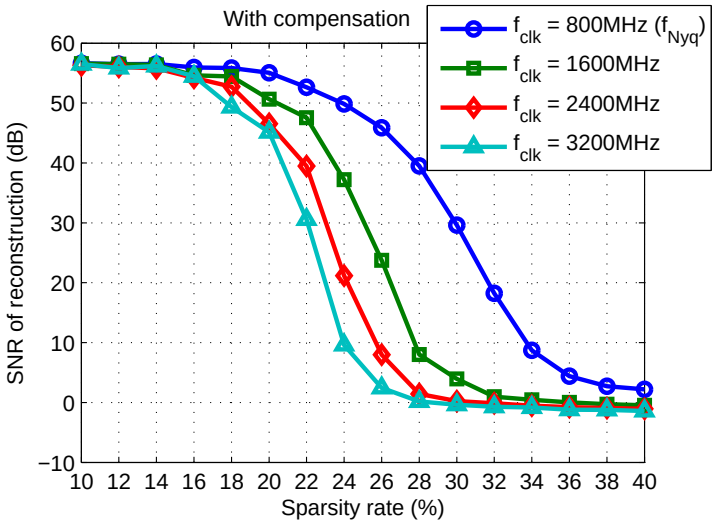

(a) With compensation

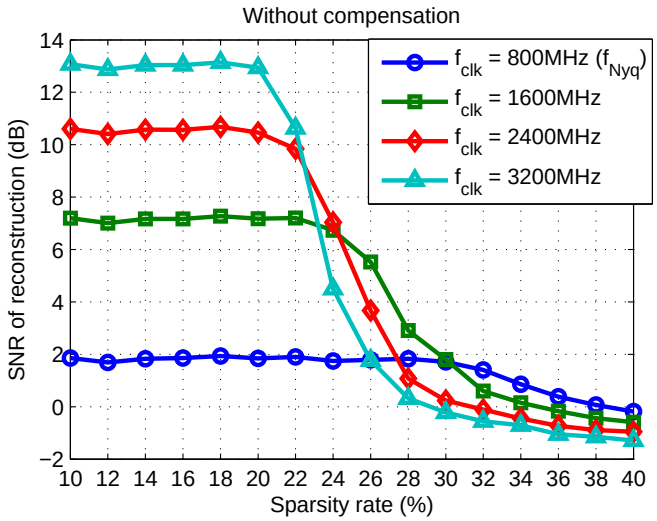

(b) Without compensation

Fig. 4.8 RMS error of overclocked PN sequences in noise-free system.

We have shown that the overclocked system is less dependent to the compensation. After this the system outcome is all compensated assuming that the pulse shape is perfectly square. Next, we study the effect of the system noise n_s Fig. 4.9 shows that the system with overclocked PN sequences is more sensitive to the noise. The non-overclocked system can sustain the noise 5dB better, at the same SNR of reconstruction. In particular, the SNR of the reconstruction drops by 3 dB from the best of 56.5 dB to 53.5 dB when the SNR of CS measurement is 23 dB and 28 dB for non-overclocked and overclocked system, respectively.

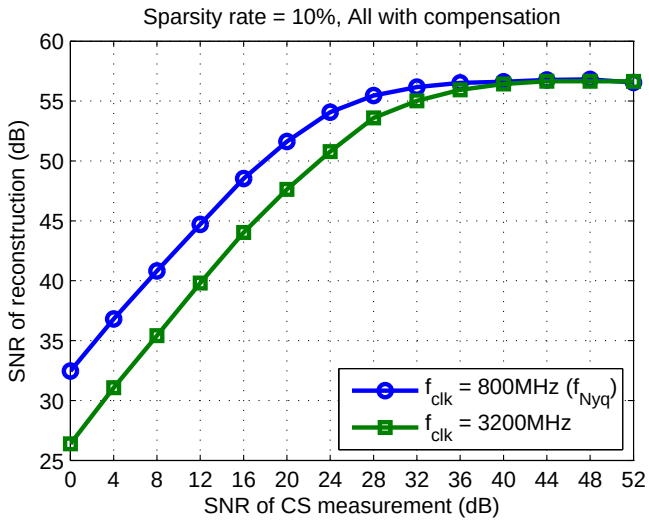

Fig. 4.9 Effect of noise-prone system.

Since jitter noise causes the pulse width to be random, the jitter noise cannot be compensated. Fig. 4.10 shows the effect of jitter to each PN chipping frequency. Higher chipping rate is unfavorably more affected by the jitter because of its shorter pulse width. Given a fixed amount of jitter rms, the jitter noise appears in larger ratio in shorter pulse width. For example, given jitter rms is 2ps it appears as 0.16% of 800MHz PN sequence's pulse width, while it is accounted as 0.64% in 3200MHz case. The SNR is slightly dropped from 56.5 dB to 53.4 dB for the non-overclocked, but decreased to 46 dB for the overclocked system.

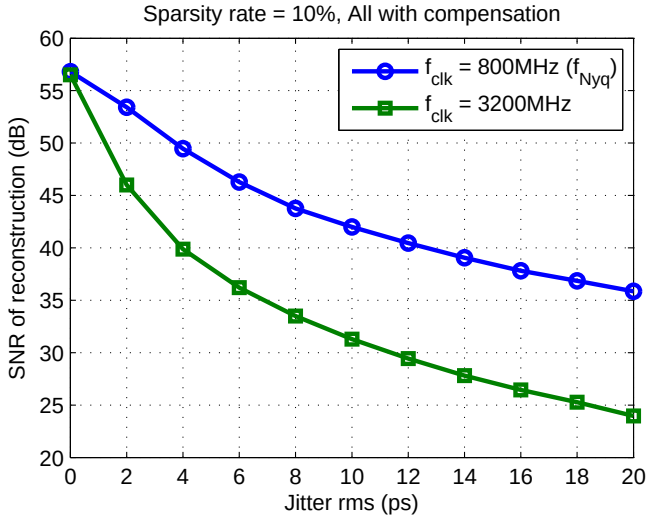

Fig. 4.10 Effect of jitter.

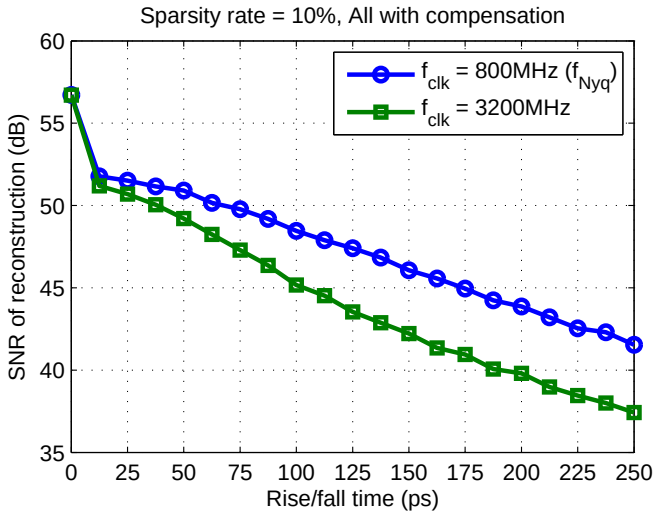

Fig. 4.11 Effect of rise/fall time.

Lastly, the impact of imperfect square pulse of PN sequence waveform is evaluated in terms of rise/fall time. Here, in order to reveal the effect of inaccurate calibration, we assume the scenario when the calibration cannot be achieved and the pulse shape is perfectly square in the compensation. Similar to jitter noise, the electronics field usually considers the amount of rise/fall time based on the state of technology regardless of the PN chipping frequency, i.e. the amount of rise/fall time is fixed at the same value on both non-overclocked and overclocked systems, and the same rise/fall time appears as larger error in overclocked systems. The result is shown in Fig. 4.11 that the non-overclocked system is more preferable to the overclocked system. For example, the SNR of reconstruction of the Nyquist-rate system is 1.7 dB better than that of the overclocked system when the rise/fall time T_r is 50 ps.

As a small remark, Fig. 4.12 shows that the overclocking is not affected from the SNR of input, and RD-based sampling provides no noise to the signal (SNR of reconstruction $\approx$ SNR of input) when the system is ideal.

In this section, we present the hardware analysis of RD-based sub-Nyquist sampling systems. The evaluation is done in the aspect of a hardware parameter and three hardware nonidealities including PN sequence chipping frequency, circuit noise, jitter, and imperfect pulse shape. Based on simulation results, the overclocked system is preferable if the compensation is not available and also when precise calibration of actual PN sequence pulse shape is burdensome. On the other hand, since the overclocking makes the system more vulnerable to a circuit noise and jitter noise, the Nyquist-rate PN sequences is

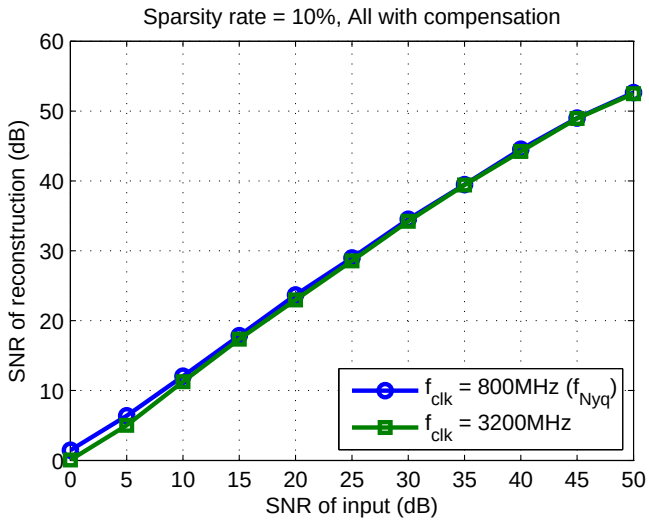

Fig. 4.12 Effect of SNR of input.

generally optimal to most implementations.

(b) MWC system

Since MWC system can sample the signal in continuous frequency domain, we evaluate the performance of MWC system for BPSK/QPSK modulated signal. The simulation is done to obtain the traditional graph of BER versus $\frac{E_b}{N_0}$. The effect of the number of channels M on BER is also studied.

Simulation setting

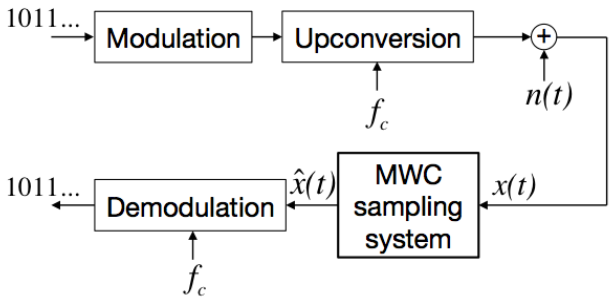

Fig. 4.13 Evaluation model of MWC sub-Nyquist sampling.

Fig. 4.13 shows the overview of the evaluation setup. The input signal is a noisy modulated signal described as

$$x(t) = \frac{2E_b}{T_{sym}} \left[I(t)\cos(2\pi f_c t) + Q(t)\sin(2\pi f_c t) \right] + n(t) \tag{4.24}$$

where E_b, T_{sym}, and f_c are the energy per bit, symbol interval, and the carrier frequency of the BPSK/QPSK signal, respectively. $I(t)$ and $Q(t)$ are the square pulse waveform representing bit streams which are drawn randomly as ± 1, where $Q_i(t) = 0$ for BPSK modulation. The modulated signal is mixed with the additive white Gaussian noise $n(t)$ with the noise spectral density N_0 corresponding to $\frac{E_b}{N_0}$. The passband bandwidth B is defined the symbol interval T_{sum} where B equals $\frac{2}{T_{sym}}$. The simulation of 3000 runs is done by using MATLAB. Each run contains 50 BPSK/QPSK symbols. The low pass filter is ideal. Table 4.2 shows the simulation settings.

Table. 4.2 Simulation settings

Parameter	Value
Passband bandwidth B	40MHz
Carrier frequency	2.2GHz
PN code length M	123
$f_p = f_s$ (normal clock frequency)	40.65MHz
f_{PN} (normal clock frequency)	5GHz
Overclocking rate	1x, 2x (labeled as Overclk)

The BER is used a performance metric defined as

$$\text{BER} = \frac{\#\text{ error bits}}{\#\text{ total bits}} \tag{4.25}$$

Simulation results

Firstly, we evaluate the system with considerably high number of channels at 60 over varying $\frac{E_b}{N_0}$. Fig. 4.14 shows the trade-off of the sub-Nyquist sampling compared to the traditional Nyquist system. Even though the sampling rate is reduced to about 49%($\frac{40.65\text{MHz}\times 60}{5\text{GHz}}$) in the normal clock case, the sub-Nyquist system requires approximately more 9 dB compared to the traditional Nyquist system, while the overclocked system requires about 7 dB higher than the traditional one. In particular, at least 13 dB is required for the overclocked system to obtain the average BER = 10^{-3}, while 15 dB is required for the non-overclocked one. Fig. 4.15 shows the performance of support detection in terms of failed rate which accounts for when the frequency location is wrong determined. Note that the failed rate of QPSK signal is better than that of BPSK signal, because the performance support detection depends on the SNR within the interest bandwidth. At the same $\frac{E_b}{N_0}$, the SNR of QPSK signal is 3 dB higher than that of BPSK

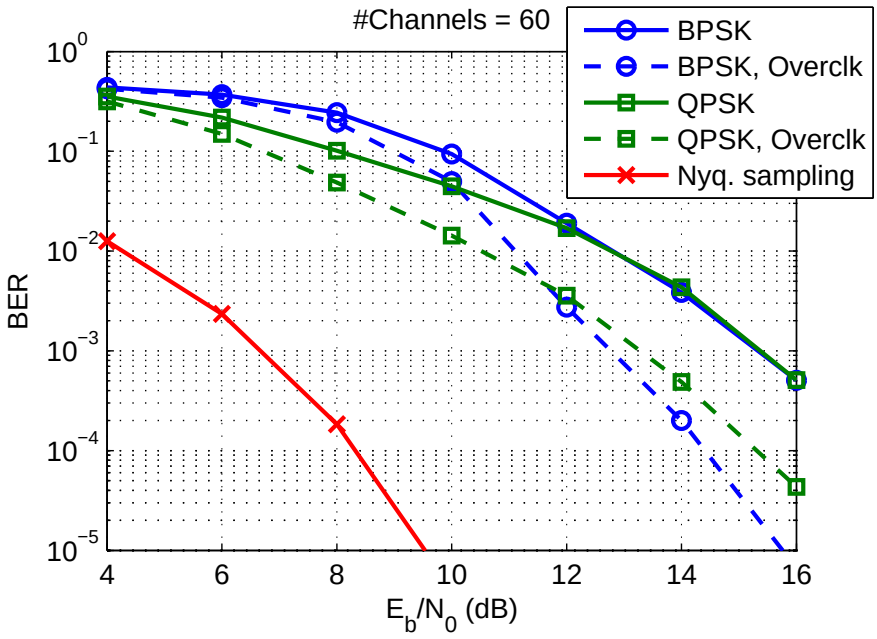

Fig. 4.14 BER over $\frac{E_b}{N_0}$.

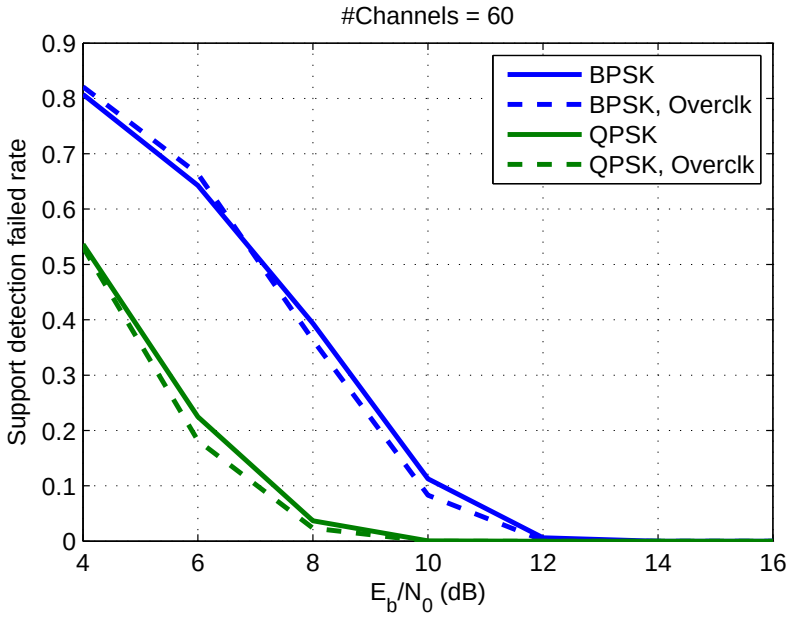

Fig. 4.15 Support detection failed rate over $\frac{E_b}{N_0}$.

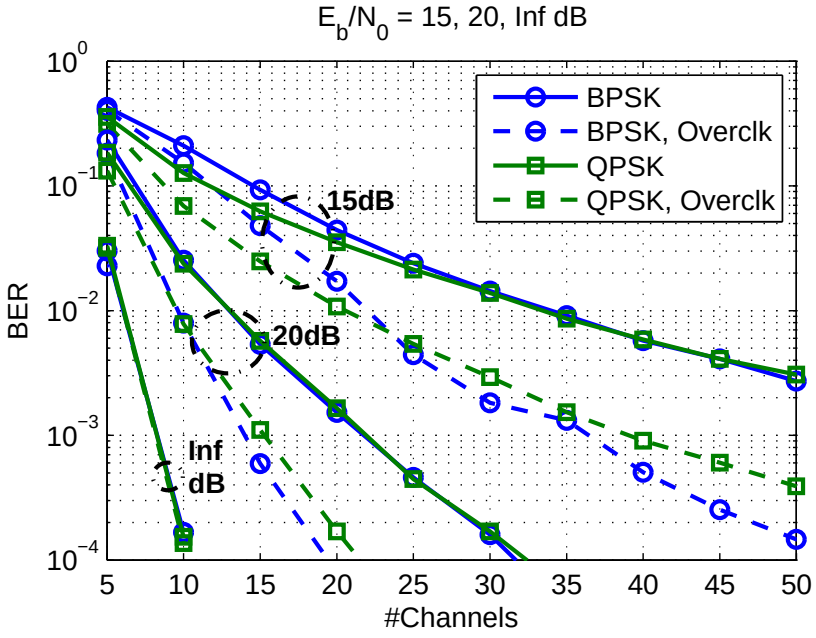

Fig. 4.16 BER over a number of channels.

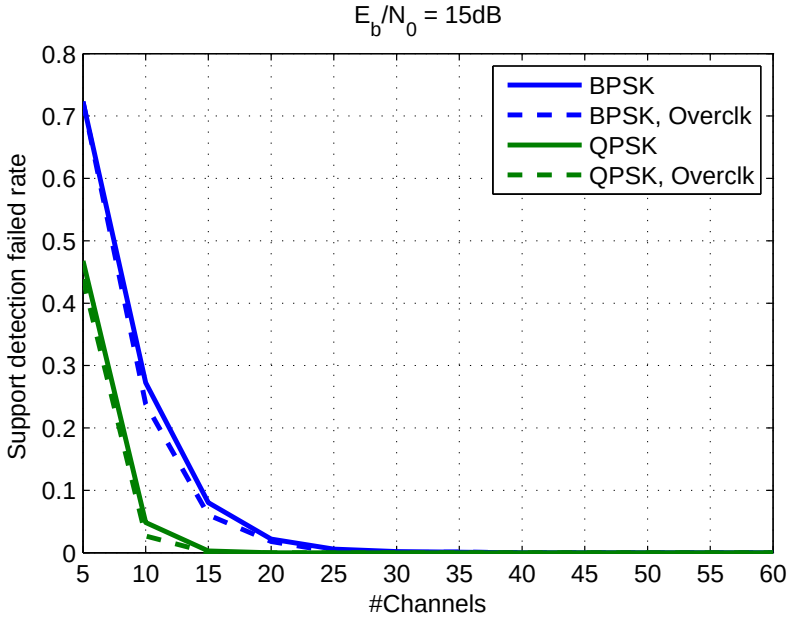

Fig. 4.17 Support detection failed rate over a number of channels ($\frac{E_b}{N_0}$ = 15 dB).

signal according to $SNR = r\frac{E_b}{N_0}$, where r is the bit rate. This also explains why at low $\frac{E_b}{N_0}$, the BER of BPSK signal is higher than that of QPSK signal.

Secondly, the BER analysis over a number of channels is done under various conditions where $\frac{E_b}{N_0}(\text{dB}) = 15, 20$, and infinity. Fig. 4.16 shows that the overclocking can reduce the number of channel required to obtain the same BER. For example, when $\frac{E_b}{N_0} = 20$ dB, if the desired BER equals 10^{-3}, 15 and 22 channels are required for the overclocked and non-overclocked system, respectively. When $\frac{E_b}{N_0} = 15$ dB, the reason that the BER of BPSK signal is higher than QPSK signal's can be explained by Fig. 4.17.

In this section, we evaluate the BER of BPSK/QPSK modulated signals by using a MWC sub-Nyquist sampling system as a receiver. The performance of the sub-Nyquist sampling is compared to that of the traditional Nyquist sampling. In addition, although the overclocking needs faster clock rate and sampling rate, it makes the system require less $\frac{E_b}{N_0}$ and less number of channels to reach a targeted BER.

4.4.2 Implementation

In this section, we implement MWC sub-Nyquist sampling system by using laboratory-instrument as a collaboration research with NTT Corporation. We aim to obtain the experimental result and compare with the simulation result as shown in Fig. 4.16.

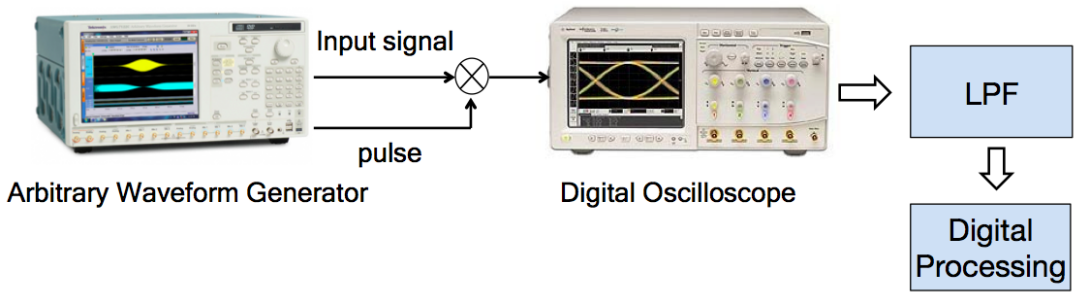

Fig. 4.18 Experiment setup of MWC sub-Nyquist sampling.

The experiment is set up as shown in Fig. 4.18. A modulated signal is generated by Arbitrary Waveform Generator (AWG) and passed through a doubled-balanced mixer manufactured by Watkins Johnson M1G. Another input of the mixer is PN sequence waveform generated from the AWG as well. The output of the mixer is recorded by an oscilloscope at 40 GHz. The low-pass filtering and sampling by low-speed ADC are done in MATLAB. While the input modulated signal is fixed, the PN sequence waveform

is changed every measurement to mimic an operation of one of parallel channels. The measurements are repeated until we get the target amount of channels.

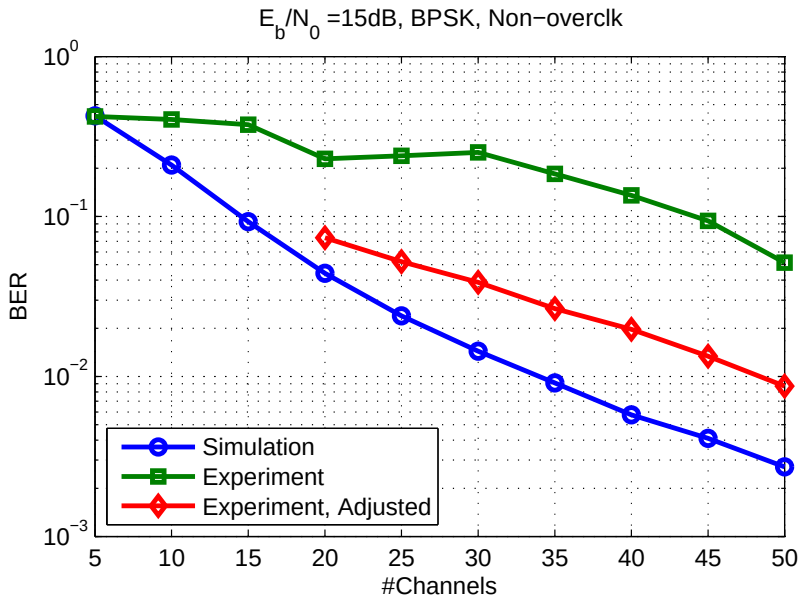

Fig. 4.19 Experimental BER over a number of channels.

Generally the parameters are set as same as those of simulation as shown in Table 4.2. However, as an initial step, we focus on only when $\frac{E_b}{N_0} = 15$ dB, the modulation is BPSK, and the PN chipping frequency is at Nyquist rate. Fig. 4.19 shows the experimental result. Due to difficulties in time synchronization, the experiment results occasionally contain severe errors and we manually remove them from our evaluation. Therefore, the experimental results are shown as two lines: with adjustment and without adjustment. The experimental result with the adjustment shows some degradation from the simulation result. This can caused by the time synchronization and the effect of the off-the-shelf mixer.

4.5 Summary

The performance of a sub-Nyquist sampling system has been evaluated intensively. We consider two sub-Nyquist sampling systems, which applies compressed sensing theory, including Random Demodulation based and Modulated Wideband Converter based system.

In RD-based system, we consider the effect of the PN chipping frequency variation along with hardware nonidealities including circuit noise, clock jitter and rise/fall of PN

sequences. The results show that the overclocked system is preferable if the compensation is not available. Otherwise, the Nyquist-rate PN sequences is generally optimal to most implementations, since the overclocking makes the system sensitive to a circuit noise, jitter noise, and rise/fall time error.

In MWC system, the evaluation in terms of bit error rate of BPSK/QPSK is achieved. The comparison between the traditional Nyquist sampling shows that the sub-Nyquist system requires significantly better signal condition, as a trade-off to reduce a sampling rate. The effect of the chipping frequency variation is also studied. The implementation on laboratory-instrument is done level to verify the simulation results.

Chapter 5

Conclusions and Future Works

5.1 Conclusions

Compressed sensing (CS) has become a hot research topic due to its promising features: reducing size of a signal by exploiting signal sparsity and incoherent measurements. This thesis explores the applications of CS in two resourced-limited wireless systems: wireless sensor network and wideband wireless communication. In both applications, the development and evaluation are based on practical aspects.

To reduce the traffic of WSN, CS is designed to suit to WSN environments. The evaluation on sensor data and implementation on sensor nodes are provided. Memory-efficient 1-bit CS which adopts a circulant random bipolar measurement matrix are applied to achieve data compression in environmental data including temperature, relative humidity, and illuminance. The results show that the scheme can reduce the traffic and save significant amount of memory compared to the conventional CS. The implementation on real sensor nodes also reveals the feasibility of the introduced scheme practically. Generally, the merits of CS-based data compression stems from CS including universal measurement matrix for most sensor data and simple encoding for small sensor nodes. However, one may consider reconstruction complexity as a demerit which is admissible in environmental monitoring application.

CS-based sub-Nyquist sampling systems for a frequency-sparse wideband signal are evaluated intensively. We study two leading architectures – random demodulation (RD) and modulated wideband converter (MWC) – based on their suitable signal model. Results show that the sub-Nyquist sampling system can achieve significant sampling rate reduction which is a main objective of applying CS. In particular, the performance of both sub-Nyquist sampling system architectures in a practical situation is discussed intensively. The overclocked RD-based system is preferable if the compensation is not available. Nyquist-rate PN sequences are generally optimal to most implementations, since the overclocking makes the RD-based system sensitive to hardware nonidealities including circuit noise, clock jitter and rise/fall of PN sequences. In MWC system, the evaluation in terms of bit error rate of BPSK/QPSK is achieved. The comparison between the traditional Nyquist sampling shows that although the sub-Nyquist system can reduce a sampling rate, it requires significantly better signal condition to obtain a target BER. Unlike RD-based system, the overclocking provides some improvement in signal reconstruction of MWC system. However, further improvements to tolerate noise and also speed up the reconstruction are required to bring CS into wide application in wideband communication area such as cognitive radio.

5.2 Future works

This section suggests approaches possibly done to accomplish more accuracy and faster speed of what have been presented in this thesis. Moreover, the application of CS on UWB impulse radio is also briefly discussed.

The reconstruction of data compression in wireless sensor networks (WSN) as presented in Chapter 3 may be improved by applying a learning basis. CS-based data compression in WSN currently applies a fixed DCT basis as a sparsifying basis in the reconstruction process. The results show that it cannot well reconstruct highly fluctuating signals as demonstrated by illuminance data. In WSN, there are also more fluctuating signals such as wind speed. A learning basis that is trained by a set of an pre collected original signal can represent a signal in more sparse manner, and therefore improves the reconstruction accuracy of CS algorithms.

Improving reconstruction speed of CS will help the practical application of CS, especially RD-based sub-Nyquist sampling system. As a disadvantage generally arisen by CS, rather than developing a new fundamental of reconstruction algorithm, distributed parallel computation concept can be used as a tool to speed up the processing. For example, GPU (graphics processing unit) programming can be a proof-of-concept implementation of an parallel computing.

As introduced in Section 1.1.2, UWB impulse radio can also be sampled by a sub-Nyquist sampling. Though CS measurement circuit and reconstruction are slightly from what present in Chapter 4, we have done an initial experiment by using a radar sensor developed by Time Domain as shown in Fig. 5.1. The radar sensor is deployed in an empty room with a large object located 5 meters apart from the sensor as shown in Fig. 5.2. Fig. 5.3 shows an example of demodulated signal which is down shifted by the carrier frequency and subtracted by a background signal. The subtraction of background signal is to reduce the effect of clutters and indoor environments. The peak represents the 5-meter object which results in the theoretical pulse delay $\frac{5\times 2}{3\times 10^8} = 33$ ns. CS-based sub-Nyquist sampling is applied to sample the demodulated signal and its performance of pulse detection is shown in Fig. 5.4. About 95% of pulses can be detected within a small error, while the sampling rate is reduced by 10 times i.e. from 4.4 GHz to 440 MHz. This initial experiment shows the feasibility of CS on noise-reduced UWB signals. Due to the low power transmission of UWB, the future work will include the development CS measurement and reconstruction scheme which improves noise tolerance.

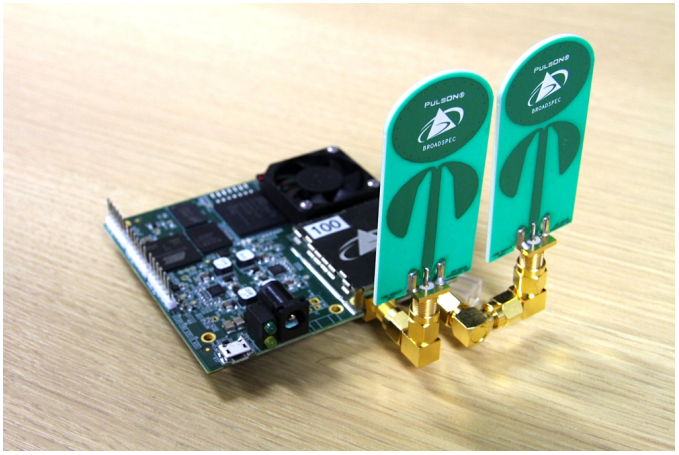

Fig. 5.1 UWB radar kit by Time Domain.

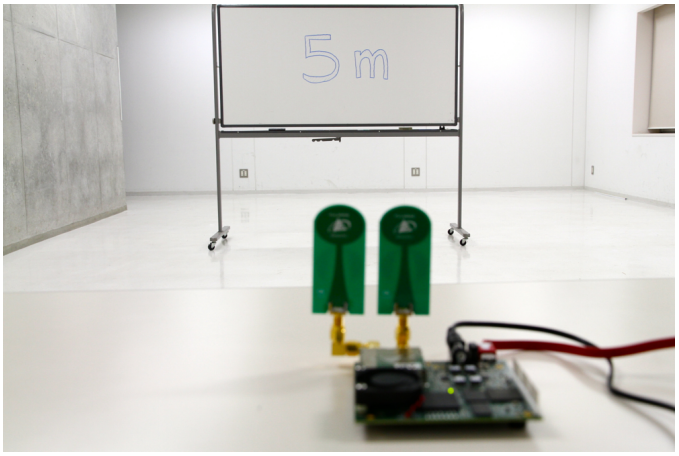

Fig. 5.2 UWB experiment setup.

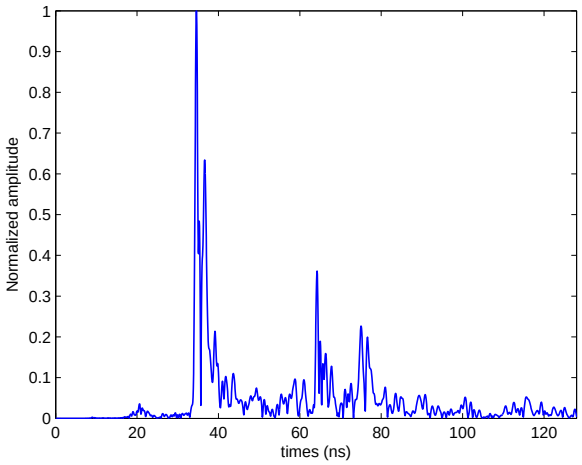

Fig. 5.3 Example of demodulated signal reflected from 5-meter object.

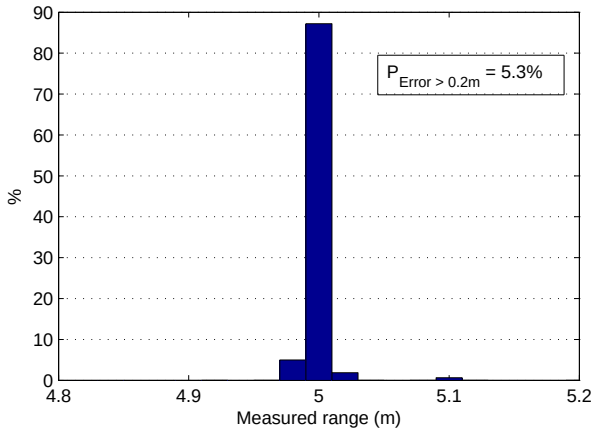

Fig. 5.4 Histogram showing the performance of pulse detection by sub-Nyquist sampling.

Acknowledgments

This research is properly achieved owing to good support from my supervisor. I would like to express my deepest gratitude to Professor Hiroyuki Morikawa for his guidances and persistent supports in regard to research and scholarships. I also appreciate Assistant Professor Doohwan Lee's advices and research guidances not only on the overview of the technical knowledge of compressed sensing but also research methodologies.

In addition, I would like to thank to committee members who spend time checking and approving this dissertation as well as giving valuable comments, and NTT Network Innovation Laboratories as a collaborative research partner who also take part in experiments in this thesis. Thank you all of my friends in Morikawa Laboratory who have been assisting me since I came to Japan. I appreciate their kind helps, warm welcome and friendly working atmosphere. Finally, I would like to gratefully thank you my family and friends who always support and inspire me in every possible ways.

Theerat Sakdejayont

February 2014

References

[1] Federal Communications Commission, "Report of the spectrum efficiency working group," Tech. Rep. 02-155, Nov. 2002.

[2] O. Abari, F. Lim, F. Chen, and V. Stojanovic, "Why analog-to-information converters suffer in high-bandwidth sparse signal applications," *IEEE Transactions on Circuits and Systems I*, vol. PP, no. 99, pp. 1–12, Feb. 2013.

[3] D. Donoho, "Compressed sensing," *IEEE Transactions on Information Theory*, vol. 52, no. 4, pp. 1289–1306, Apr. 2006.

[4] N. Kimura and S. Latifi, "A survey on data compression in wireless sensor networks," in *Proceedings of International Conference on Information Technology: Coding and Computing*, vol. 2, pp. 8–13, Las Vegas, NV, Apr. 2005.

[5] Federal Communications Commission, "First report and order, revision of part 15 of the commission's rules regarding ultra-wideband transmission systems," Tech. Rep. 02-48, Apr. 2002.

[6] C. Shannon, "Communication in the presence of noise," *Proceedings of the Institute of Radio Engineers*, vol. 37, no. 1, pp. 10–21, Jan. 1949.

[7] R. Walden, "Analog-to-digital converter survey and analysis," *IEEE Journal on Selected Areas in Communications*, vol. 17, no. 4, pp. 539–550, Apr. 1999.

[8] B. Le, T. Rondeau, J. Reed, and C. Bostian, "Analog-to-digital converters," *IEEE Signal Processing Magazine*, vol. 22, no. 6, pp. 69–77, Dec. 2005.

[9] B. Murmann, "A/D converter trends: Power dissipation, scaling and digitally assisted architectures," in *Proceedings of IEEE Custom Integrated Circuits Conference*, pp. 105–112, San Jose, CA, Sep. 2008.

[10] M. Mishali and Y. Eldar, "Sub-Nyquist sampling: Bridging theory and practice," *IEEE Signal Processing Magazine*, vol. 28, no. 6, pp. 98–124, Nov. 2011.

[11] J. Laska, S. Kirolos, M. Duarte, T. Ragheb, R. Baraniuk, and Y. Massoud, "Theory and implementation of an analog-to-information converter using random demodulation," in *Proceedings of IEEE International Symposium on Circuits and Systems*, pp. 1959–1962, New Orleans, LA, May 2007.

[12] J. Tropp, J. Laska, M. Duarte, J. Romberg, and R. Baraniuk, "Beyond Nyquist: Efficient sampling of sparse bandlimited signals," *IEEE Transactions on Information Theory*, vol. 56, no. 1, pp. 520–544, Jan. 2010.

[13] Z. Yu, S. Hoyos, and B. Sadler, "Mixed-signal parallel compressed sensing and reception for cognitive radio," in *Proceedings of IEEE International Conference on Acoustics, Speech and Signal Processing*, pp. 3861–3864, Las Vegas, NV, Mar. 2008.

[14] X. Chen, Z. Yu, S. Hoyos, B. Sadler, and J. Silva-Martinez, "A sub-Nyquist rate sampling receiver exploiting compressive sensing," *IEEE Transactions on Circuits and Systems I*, vol. 58, no. 3, pp. 507–520, Mar. 2011.

[15] E. Candès, "Compressive sampling," in *Proceedings of the International Congress of Mathematicians*, pp. 1433–1452, Madrid, Spain, Aug. 2006.

[16] E. Candes, J. Romberg, and T. Tao, "Stable signal recovery from incomplete and inaccurate measurements," *Communications on pure and applied mathematics*, vol. 59, no. 8, pp. 1207–1223, Aug. 2006.

[17] M. Grant and S. Boyd, "CVX: Matlab software for disciplined convex programming, version 2.0 beta," Available at http://cvxr.com/cvx, Sep. 2013.

[18] M. Figueiredo, R. Nowak, and S. Wright, "Gradient projection for sparse reconstruction: Application to compressed sensing and other inverse problems," *IEEE Journal of Selected Topics in Signal Processing*, vol. 1, no. 4, pp. 586–597, Dec. 2007.

[19] A. C. Gilbert, M. J. Strauss, J. A. Tropp, and R. Vershynin, "One sketch for all: Fast algorithms for compressed sensing," in *Proceedings of the 39th Annual ACM Symposium on Theory of Computing*, pp. 237–246, San Diego, CA, Jun. 2007.

[20] J. Tropp and A. Gilbert, "Signal recovery from random measurements via orthogonal matching pursuit," *IEEE Transactions on Information Theory*, vol. 53, no. 12, pp. 4655–4666, Dec. 2007.

[21] I. Daubechies, M. Defrise, and C. De Mol, "An iterative thresholding algorithm for linear inverse problems with a sparsity constraint," *Communications on pure and applied mathematics*, vol. 57, no. 11, pp. 1413–1457, Nov. 2004.

[22] M. Duarte, M. Davenport, D. Takhar, J. Laska, T. Sun, K. Kelly, and R. Baraniuk, "Single-pixel imaging via compressive sampling," *IEEE Signal Processing Magazine*, vol. 25, no. 2, pp. 83–91, Mar. 2008.

[23] M. Lustig, D. Donoho, and J. M. Pauly, "Sparse MRI: The application of compressed sensing for rapid MR imaging," *Magnetic resonance in medicine*, vol. 58, no. 6, pp. 1182–1195, Dec. 2007.

[24] G. Hennenfent and F. J. Herrmann, "Simply denoise: Wavefield reconstruction via jittered undersampling," *Geophysics*, vol. 73, no. 3, pp. V19–V28, May-Jun. 2008.

[25] M. Herman and T. Strohmer, "High-resolution radar via compressed sensing," *IEEE Transactions on Signal Processing*, vol. 57, no. 6, pp. 2275–2284, Jun. 2009.

[26] J. Bobin, J.-L. Starck, and R. Ottensamer, "Compressed sensing in astronomy," *IEEE Journal of Selected Topics in Signal Processing*, vol. 2, no. 5, pp. 718–726, Dec. 2008.

[27] C. Karakus, A. Gurbuz, and B. Tavli, "Analysis of energy efficiency of compressive sensing in wireless sensor networks," *IEEE Sensors Journal*, vol. 13, no. 5, pp. 1999–2008, May 2013.

[28] P. Boufounos and R. Baraniuk, "1-bit compressive sensing," in *Proceedings of 42nd Annual Conference on Information Sciences and Systems*, Princeton, NJ, Mar. 2008.

[29] W. Bajwa, J. Haupt, G. Raz, S. Wright, and R. Nowak, "Toeplitz-structured compressed sensing matrices," in *Proceedings of IEEE/SP 14th Workshop on Statistical Signal Processing*, pp. 294–298, Madison, WI, Aug. 2007.

[30] H. Mamaghanian, N. Khaled, D. Atienza, and P. Vandergheynst, "Compressed sensing for real-time energy-efficient ECG compression on wireless body sensor nodes," *IEEE Transactions on Biomedical Engineering*, vol. 58, no. 9, pp. 2456–2466, Sep. 2011.

[31] A. Dixon, E. Allstot, D. Gangopadhyay, and D. Allstot, "Compressed sensing system considerations for ECG and EMG wireless biosensors," *IEEE Transactions on Biomedical Circuits and Systems*, vol. 6, no. 2, pp. 156–166, Apr. 2012.

[32] F. Chen, A. Chandrakasan, and V. Stojanovic, "Design and analysis of a hardware-efficient compressed sensing architecture for data compression in wireless sensors," *IEEE Journal of Solid-State Circuits*, vol. 47, no. 3, pp. 744–756, Feb. 2012.

[33] F. Chen, F. Lim, O. Abari, A. Chandrakasan, and V. Stojanovic, "Energy-aware design of compressed sensing systems for wireless sensors under performance and reliability constraints," *IEEE Transactions on Circuits and Systems I: Regular Papers*, vol. 60, no. 3, pp. 650–661, Feb. 2013.

[34] Z. Zhang, T.-P. Jung, S. Makeig, and B. Rao, "Compressed sensing for energy-efficient wireless telemonitoring of noninvasive fetal ECG via block sparse bayesian learning," *IEEE Transactions on Biomedical Engineering*, vol. 60, no. 2, pp. 300–309, Feb. 2013.

[35] W. Bajwa, J. Haupt, A. Sayeed, and R. Nowak, "Joint source-channel communication for distributed estimation in sensor networks," *IEEE Transactions on Information Theory*, vol. 53, no. 10, pp. 3629–3653, Oct. 2007.

[36] C. Luo, F. Wu, J. Sun, and C. Chen, "Compressive data gathering for large-scale wireless sensor networks," in *Proceedings of the 15th Annual International Conference on Mobile Computing and Networking*, pp. 145–156, Beijing, China, Sep. 2009.

[37] J. Luo, L. Xiang, and C. Rosenberg, "Does compressed sensing improve the throughput of wireless sensor networks?" in *Proceedings of IEEE International Conference on Communications*, pp. 1–6, Cape Town, South Africa, May 2010.

[38] W. Wang, M. Garofalakis, and K. Ramchandran, "Distributed sparse random projections for refinable approximation," in *Proceedings of 6th International Symposium on Information Processing in Sensor Networks*, pp. 331–339, Cambridge, MA, Apr. 2007.

[39] M. Suzuki, Y. Yamashita, and H. Morikawa, "Low-power, end-to-end reliable collection using Glossy for wireless sensor network," in *Proceedings of IEEE 77th Vehicular Technology Conference*, Dresden, Germany, Jun. 2013.

[40] H. Rauhut, J. Romberg, and J. Tropp, "Restricted isometries for partial random circulant matrices," *Applied and Computational Harmonic Analysis*, vol. 32, no. 2, pp. 242–254, Mar. 2012.

[41] T. Shimojo, Y. Tashiro, T. Morito, M. Suzuki, D. Lee, I. Kondo, N. Fukuda, and H. Morikawa, "A leaf area index visualization method using wireless sensor networks," in *Proceedings of SICE Annual Conference*, Nagoya, Japan, Sep. 2013.

[42] L. Jacques, J. Laska, P. Boufounos, and R. Baraniuk, "Robust 1-bit compressive sensing via binary stable embeddings of sparse vectors," *IEEE Transactions on Information Theory*, vol. 59, no. 4, pp. 2082–2102, Apr. 2013.

[43] M. Mishali and Y. Eldar, "From theory to practice: Sub-Nyquist sampling of sparse wideband analog signals," *IEEE Journal of Selected Topics in Signal Processing*, vol. 4, no. 2, pp. 375–391, Apr. 2010.

[44] T. Ragheb, J. N. Laska, H. Nejati, S. Kirolos, R. G. Baraniuk, and Y. Massoud, "A prototype hardware for random demodulation based compressive analog-to-digital conversion," in *Proceedings of 51st Midwest Symposium on Circuits and Systems*, pp. 37–40, Knoxville, TN, Aug. 2008.

[45] X. Chen, E. Sobhy, Z. Yu, S. Hoyos, J. Silva-Martinez, S. Palermo, and B. Sadler, "A sub-Nyquist rate compressive sensing data acquisition front-end," *IEEE Journal on Emerging and Selected Topics in Circuits and Systems*, vol. 2, no. 3, pp. 542–551, Sep. 2012.

[46] T. S. Murray, P. O. Pouliquen, and A. G. Andreou, "Design of a parallel sampling encoder for analog to information (A2I) converters: Theory, architecture and CMOS implementation," *Electronics*, vol. 2, no. 1, pp. 57–79, Mar. 2013.

[47] M. Mishali, Y. Eldar, O. Dounaevsky, and E. Shoshan, "Xampling: Analog to digital at sub-Nyquist rates," *IET Circuits, Devices & Systems*, vol. 5, no. 1, pp. 8–20, Jan. 2011.

[48] W. J. Black and D. Hodges, "Time interleaved converter arrays," *IEEE Journal of Solid-State Circuits*, vol. 15, no. 6, pp. 1022–1029, Dec. 1980.

[49] R. Vaughan, N. Scott, and D. White, "The theory of bandpass sampling," *IEEE Transactions on Signal Processing*, vol. 39, no. 9, pp. 1973–1984, Sep. 1991.

[50] Y.-P. Lin and P. Vaidyanathan, "Periodically nonuniform sampling of bandpass signals," *IEEE Transactions on Circuits and Systems II: Analog and Digital Signal Processing*, vol. 45, no. 3, pp. 340–351, Mar. 1998.

[51] J. Laska, S. Kirolos, Y. Massoud, R. Baraniuk, A. Gilbert, M. Iwen, and M. Strauss, "Random sampling for analog-to-information conversion of wideband signals," in *Proceedings of IEEE Dallas/CAS Workshop on Design, Applications, Integration and Software*, pp. 119–122, Richardson, TX, Oct. 2006.

[52] M. Mishali and Y. Eldar, "Blind multiband signal reconstruction: Compressed sensing for analog signals," *IEEE Transactions on Signal Processing*, vol. 57, no. 3, pp. 993–1009, Feb. 2009.

[53] J. Tropp, M. Wakin, M. Duarte, D. Baron, and R. Baraniuk, "Random filters for compressive sampling and reconstruction," in *Proceedings of IEEE International Conference on Acoustics, Speech and Signal Processing*, vol. 3, pp. III872–III875, Toulouse, France, Mar. 2006.

[54] Y. Eldar, "Compressed sensing of analog signals in shift-invariant spaces," *IEEE Transactions on Signal Processing*, vol. 57, no. 8, pp. 2986–2997, Aug. 2009.

[55] S. Kirolos, J. Laska, M. Wakin, M. Duarte, D. Baron, T. Ragheb, Y. Massoud, and R. Baraniuk, "Analog-to-information conversion via random demodulation," in *Proceedings of IEEE Dallas/CAS Workshop on Design, Applications, Integration and Software*, pp. 71–74, Richardson, TX, Oct. 2006.

[56] J. Yoo, S. Becker, M. Loh, M. Monge, E. Candes, and A. Emami-Neyestanak, "A 100MHz 2GHz 12.5x sub-Nyquist rate receiver in 90nm CMOS," in *Proceedings of IEEE Radio Frequency Integrated Circuits Symposium*, pp. 31–34, Montreal, QC, Jun. 2012.

Publications

国際会議

[1] T. Sakdejayont, D. Lee, Y. Peng, Y. Yamashita, and H. Morikawa, “Evaluation of memory-efficient 1-bit compressed sensing in wireless sensor networks,” in Proceedings of the IEEE Region 10 Humanitarian Technology Conference 2013, pp.326–329 Sendai, Japan, Aug. 2013.

全国大会

[2] T. Sakdejayont, D. Lee, and H. Morikawa, “Analysis of overclocked PN sequences in sub-Nyquist sampling for wideband sparse signals,” 電子情報通信学会ソサイエティ大会，B-17-11，Sep. 2013.

[3] T. Sakdejayont, D. Lee, H. Morikawa, T. Yamada, H. Shiba, H. Sasaki, and T. Nakagawa, “Evaluation of sub-Nyquist sampling for BPSK/QPSK signals sparsely located in wideband spectrum,” 電子情報通信学会総合大会，Mar. 2014.

[4] 笹木裕文, 山田貴之, 芝 宏礼, 中川匡夫, 李 斗煥, サクデーシャヨン　ティラット, 森川 博之, “オーバークロックを用いたアナログ圧縮センシング装置のサンプリング周波数に関する一検討,” 電子情報通信学会総合大会，Mar. 2014.

特許出願

[5] 李 斗煥, サクデーシャヨン ティラット, 森川 博之, 山田 貴之, 芝 宏礼, 笹木 裕文, 中川 匡夫, “信号処理システム及び信号処理方法,” 出願予定 , Mar. 2014.